TAMPEREEN TEKNILLINEN YLIOPISTO
TAMPERE UNIVERSITY OF TECHNOLOGY

Mohammad Kazemi Pilehrood

Nanostructured Fiber Materials and Composites for Tissue Engineering

Julkaisu 1432 • Publication 1432

Tampere 2016

Tampereen teknillinen yliopisto. Julkaisu 1432
Tampere University of Technology. Publication 1432

Mohammad Kazemi Pilehrood

Nanostructured Fiber Materials and Composites for Tissue Engineering

Thesis for the degree of Doctor of Science in Technology to be presented with due permission for public examination and criticism in Festia Building, Auditorium Pieni Sali 1, at Tampere University of Technology, on the 9th of December 2016, at 12 noon.

Tampereen teknillinen yliopisto - Tampere University of Technology
Tampere 2016

ISBN 978-952-15-3843-8 (printed)
ISBN 978-952-15-3893-3 (PDF)
ISSN 1459-2045

ABSTRACT

The demand for organ transplantation is increased day by day, highlighting the necessity for the development of tissue engineering as a part of strategic solution in medical treatments. Nanotechnology has brought a possibility to introduce materials, architectures and specific topographies required for the closet analogies in extracellar matrix (ECM) in native tissue. Among different nanostructured materials, electrospun nanofibers are recommended as an appropriate scaffold for tissue engineering due to their structural, biomedical and biophysical properties.

The aim of this thesis was to study the properties of electrospun nanofibers as scaffolds in tissue engineering. To this end, we first studied electrospinning mechanism as a nanofabrication method for the preparation of electrospun nanofibers. Secondly, the structural characteristics of electrospun nanofibers in different morphological conditions were observed by image analysis. In the third step, the comparative study was established between these structural characteristics and the viability of cells. And finally, the effects of nanofiber coating in viability, proliferation and differentiation of mesenchymal stem cells were discussed.

Polyacrylonitrile (PAN) nanofibers and carbon nanotube (CNT) reinforced PAN nanofibers were electrospun successfully. A polymer plasticiser, ethylene carbonate (EC), was added into the PAN/CNT solutions. It was observed that increasing the polymer concentration led to a reduction of beads density and an increase in the diameter of the PAN nanofibers. The fiber diameters also increased as a result of the addition of CNTs below the electrical percolation threshold. It was found that the inclusion of EC permits changes in the morphological characteristics of the PAN/CNT nanocomposite fiber regardless of the effects of its conductivity and viscosity.

3D nanofibrous chitosan-polyethylene oxide (PEO) scaffolds were fabricated by electrospinning using different processing parameters. The structural characteristics, such as pore size, overall porosity, pore interconnectivity, and scaffold percolative efficiency (SPE), were observed by using detailed image analysis. Mouse fibroblast cells (L929) were cultured in RPMI for 2 days in the presence of various samples of nanofibrous chitosan/PEO scaffolds. Cell attachment and the corresponding mean viability were enhanced from 50% to 110% compared to that of a control even at packed morphologies of scaffolds constituted from pores with nanoscale diameter. To elucidate the correlation between structural characteristics within the depth of the scaffolds' profile and cell viability, a comparative analysis was proposed. This analysis revealed that larger fiber diameters and pore sizes can enhance cell viability. On the contrary, increasing the other structural elements such as overall porosity and interconnectivity due to a simultaneous reduction in fiber diameter and pore size through the electrospinning process can reduce the viability of cells. In addition, it was found that manipulation of the processing parameters in electrospinning can compensate for the

effects of packed morphologies of nanofibrous scaffolds and can thus potentially improve the infiltration and viability of cells.

We present a new hybrid scaffold constructed by coating electrospun chitosan/polyethylene oxide (PEO) nanofibers on commercial BioTek polystyrene (PS) scaffold obtained from Sigma Aldrich. The viability and proliferation rate of mesenchymal stem cells (MSCs) seeded on micro-nano structured hybrid scaffold (MNHS) and commercial PS scaffolds were analyzed using the MTT assay. The results of the MTT assay revealed a higher degree of viability and proliferation rate in MSCs seeded on MNHS compared with the commercial PS scaffold. DAPI images also confirmed the higher degree of attachment and viability of MSCs seeded on MNHS. Moreover, MSCs on both scaffolds differentiated to osteoblasts and adipocytes cells, as reflected by the images obtained from Alizarin Red and Oil Red-O staining. Alkaline phosphatase activity (ALP) and calcium content assays revealed that the MNHS has a higher potential for osteogenic differentiation than the commercial scaffold. To quantify the osteoblast and adipocyte gene expression, quantitative RT-PCR was carried out for MNHS, commercial scaffold and Tissue culture polystyrene (TCPS). It was found that MNHS can express a higher level of Runt-related transcription factor 2 (Runx2), osteonectin and osteocalcin in osteogenic differentiation as well as increased expression of PPARγ and UCP-1 in adipogenic differentiation. The enhancement of the attachment, viability and proliferation as well as bi-lineage differentiation may result from the biochemical and structural analogies of MNHS to native ECM. Furthermore, it was observed that biocompatible MNHS scaffold can potentially be utilized as a suitable scaffold for bone and connective tissue engineering.

PREFACE

I wish to express my sincere gratitude to my supervisors Prof. Ali Harlin and Prof. Jurkka Kuusipalo for their guidance during completion of this thesis. Besides my supervisors, I would like to thanks all co-authors of my papers, especially, Prof. Sadeghi- Aliabadi from School of Pharmacy, Isfahan University of Medical Sciences and Prof. Perrti Nousiainen from Department of Materials Science, Tampere University of Technology. My sincere thanks go to my parents who have supported me throughout my life. This thesis was carried in the Department of Materials Science, Tampere University of Technology during 2008-2015.

Mohammad Kazemi Pilehrood

December 2015

CONTENTS

ABSTRACT II

PREFACE IV

CONTENT V

LIST OF ORGINAL PUBLICATION VII

LIST OF SYMBOLS AND ABBREVIATIONS VIII

1 INTRODUCTION **1**

2 NANOSTRUCTURED MATERIALS IN TISSUE ENGINEERING **4**

2.1 Nanotopography and Its Interactions with Cells 4
2.2 Electrospun Nanofibers as a Tissue Scaffolds 6
2.3 Structural Characteristics of Nanofibrous Scaffolds and Cells Viability 6
2.4 Chitosan Nanofiberous scaffolds 7
2.5 Simulation of Structural properties of Nanofibrous Scaffolds 8
2.6 Nanofibrous Scaffolds and Stem Cells 9

3 MATERIALS AND METHODS **11**

3.1 Materials 11

3.2 Electrospinning

3.2.1 Electrospinning of PAN Nanofibers and PAN/CNT Nanocomposite Fibers 11
3.2.2 Electrospinning of Chitosan/PEO Nanofibers 12
3.2.3 Fabrication of Mico/Nanostructured Hybrid Scaffold 13

3.3 Characterization of Electrospun Nanofibers and scaffolds 13

3.3.1 Morphological Observations 14
3.3.2 Viscometery and Electrical Conductivity measurement 14
3.3.3 Structural Characteristics Simulation by Image Analysis 14
3.3.3.1 Segmentation Procedure 15
3.3.3.2 Porosity Characteristics Measurement 16
3.3.3.3 Layered Porosity Characteristics 17
3.3.3.4 Intrinsic Structural Properties and Their Relation to Depth Filtration Elements 19
3.3.3.5 Method Implementation and Validation 22

3.3.4 Biological Characterizations 22
3.3.4.1 L929 Cells Viability(MTT Assay) 22
3.3.4.2 MSCs Viability(MTT Assay) 22
3.3.4.3 DAPI Staining 23
3.3.4.4 In Vitro Differentiation into Ostoblasts and Adipocytes 23
3.3.4.5 Alkaline Phosphatase Activity 23
3.3.4.6 Calcium Content Assay 23

3.3.4.7 Quantitative RT-PCR....24
3.3.5 Statistical Analysis....24

4 RESULTS AND DISSCUTION....25

4.1. Solution properties of PAN/CNT....25
4.2. Effect of polymer concentration and carbon nanotube on morphology of PAN fibres....26
4.3 Effect of Ethylene Carbonate on Morphology of PAN/CNT Nanofibres....28
4.4 The Relation between Morphological Variations and Structural Characteristic....30
4.5 Evaluation of Depth Filtration (infiltration) and Optimal Pore Size (OPS) in Nanofibrous Membrane...33
4.6 Relation between Structural Characteristics of Chitosan Nanofibrous Scaffold and Cell Viability....34
4.7 Effect of Nanofiber Coating on Viability and Proliferation Rate of Mesenchymal Stem Cells....36
4.8 Effect of Nanofiber Coating on Differentiations of Mesenchymal Stem Cells....38
4.8.1 Effect of Nanofiber Coating on Osteogenic Differentiations of Mesenchymal Stem Cells....38
4.8.2 Effect of Nanofiber Coating on Adipogenic Differentiations of Mesenchymal Stem Cells....40

5 CONCLUSIONS....42

REFERENCES....43

SUMMARIES OF PAPERS....55

LIST OF ORIGINAL PUBLICATIONS

Published papers:

1. Kazemi Pilehrood, M., Heikkilä, P., & Harlin, A. (2012). Preparation of Carbon Nanotube Embedded in Polyacrylonitrile (PAN) Nanofibre Composites by Electrospinning Process. *AUTEX Research Journal*, *12*, 1-6.

2. Kazemi Pilehrood, M., Heikkilä, P., & Harlin, A. (2013). Simulation of Structural Characteristics and Depth Filtration Elements in Interconnected Nanofibrous Membrane Based on Adaptive Image Analysis. *World Journal of Nano Science and Engineering*, *3*, 6-16. (Invited nominee because of this paper for the Eni Award 2014 by Award Scientific Secretariat, Milan, Italy)

3. Kazemi Pilehrood, M., Dilamian, M., Mirian, M., Sadeghi-Aliabadi, H., Maleknia L., Nousiainen, P., & Harlin, A. (2014). Nanofibrous Chitosan- Polyethylene Oxide (PEO) Engineered Scaffolds: A Comparative Study between Simulated Structural Characteristics and Cells Viability. *BioMed Research International, Volume 2014, Article ID: 438065.*

4. Kazemi Pilehrood. M., Atashi. A., Sadegh-Aliabadi,H., Nousiainen, P., & Harlin, A. (2016). 3D Micro-Nano Structured Hybrid Scaffolds: An Investigation on the Role of Nanofibers Coating in Viability, Proliferation and Differentiations of Seeded Mesenchymal Stem Cells. *Journal of Nanoscience and Nanotechnology, 16,* 9000-9007.

AUTHOR'S CONTRIBUTION

The author proposed the papers and performed the experimental parts, interpreted the results and was responsible for the preparation of the original papers. The co-authors commented the papers, and made suggestions for the improvement of the manuscript. The biological parts were done in Department of Pharmaceutical Chemistry, Isfahan University of Medical Sciences. The co-authors acted as supervisors, commentators and trainer of biological tests during the preparation of the fourth paper.

LIST OF SYMBOLS AND ABBREVIATIONS

Symbols

T(i,j)	local threshold
P	overall porosity
O_{50}	half way open area
H	hill slop
F(x)	best fitted curve for layered porosities
$E(d_p)$	fractural filtration efficiency
$C_1\ (d_p)$	upstream concentration
$C_2\ (d_p)$	downstream concentration
α	constant filtration efficiency
E	filtration
P	permeation

Abbreviations

ECM	extracellar matrix
PAN	polyacrylonitrile
CNT	carbon nanotube
EC	ethylene carbonate
PEO	polyethylene oxide
SPE	scaffold percolative efficiency
PS	polystyrene
MNHS	micro-nano structured hybrid scaffold
MSC	mesenchymal stem cell

ALP	alkaline phosphatase activity
Runx2	runt-related transcription factor 2
TCPS	tissue culture polystyrene
OPS	optimal pore size
SEM	scanning electron microscopy
hMCS	human mesenchymal stem cell
DMF	N, N-Dimethylformamide
MWCNT	multi-wall carbon nanotubes
CCVD	chemical vapour deposition
DD	degree of deacetylation
GA	glutaraldehyde
FESEM	field emission scanning electron microscopy
UV	ultra violet
PBS	phosphate buffer
OD	optical density
Cs	chitosan
Ca^{2+}	calcium ion
SD	standard deviation

1 INTRODUCTION

Over just a few decades, organ transplantation has undergone rapid progress from clinical trials to realistic medical treatments. Nonetheless, waiting lists of tissue repair have remained a major challenge due to the lack of availability of donors. This is due to the imbalance between the demands and availability of the required tissue for transplantation. From a statistical standpoint, almost a quarter of patients in United State are waiting for suitable organ donor [1-3], revealing the significance of developing the tissue engineering as a part of alternative strategic solution.

Tissue engineering is a sub-discipline of biomaterials dealing with cell biology, engineering and materials science, so as to develop biological substitutes to repair, restore and regenerate different tissues [4-5]. In general, cells, scaffolds and growth-stimulating signals are three main supportive elements to be discussed in this field [6]. In brief, to perform an autologous implant, cells are removed from donor tissue and cultured in an appropriate biological environment. This environment is surrounded by nanostructured protein fibers forming three dimensional porous structures known as extracellular matrix (ECM). ECM proteins exhibit nanoscale constituters postulated to be involved in cell-matrix signaling [7]. This is because of the anchorage dependent characteristics of normal cells require a supporting material for cultivation. [1] Accordingly, one of the significant challenges in tissue engineering is the introduction a supporting structure with close resemblance to native ECM known as a scaffold. Theses analogies may involve biochemical, biophysical and structural properties, leading to cellular attachment, viability, proliferation and differentiation.

It is noteworthy that nanotopography is not limited only to the basement membrane, but individual cells also interact with native topography through a different mechanism known as contact guidance [7]. This is an example of a naturally occurring phenomenon modulated by ECM proteins, and is considered to have a major impact on cellular migration [7, 8]. Contact guidance plays a significant role in migration of individual or all groups of cells or tissue whereas it can influence efficient organelle formation, such as axonal guidance and growth cone motility [7, 9-10]. Although, there are many types of ECMs specific tissue, originating from different components, the roles of ECM can be classified in five major categories [6]:

a) Provides structural support for cellular attachment, migration, proliferation and differentiation both in vivo and in vitro; b) Contributes mechanical characteristics of tissues such as mechanical strength, rigidity and stiffness; c) Provides biological cues for cells to respond to microenvironment; d) Acts as a reservoir of growth factors; e) Provides the required flexibility for remodeling of tissue based on its dynamic processes such as vascularization or wound healing procedure.

The aforementioned items are attributed to the function of native ECM whereas a desirable scaffold is determined based on having such characteristics correspondingly in engineered tissue. The introduction of a customized scaffold fulfilling these multifunctions and properties is still the major obstacle and requires special biomaterials and fabrication methods. The architecture of the scaffold should offer appropriate porosity, required for mass transport phenomena such as cellular infiltration, nutrient delivery, oxygen permeation, waste removal and vascularisation [6-11].

The biomaterials should be biodegradable upon implantation with a rate of degradation which preservs the scaffold structure until new matrix is produced in the developing tissue. The mechanical properties of biomaterials used in the scaffold should match with the host tissue and maintain the stability of the scaffold during the metabolic transport. The biomaterials used in the scaffold may have biological cues such as cell adhesive ligands or physical cues such as appropriate surface topography, leading to facilitation and manipulation of cellular activities. The scaffold should be cyto and tissue compatible in a way that serves to support cellular attachment, proliferation and differentiation both in vivo and in vitro. [6]

Previously, the structure of customized scaffolds was designed at the macroscopic scale; however, the results of the cell cultivation were not completely successfully [12]. Now, it has been confirmed that the scaffold should be modeled on a tissue specific-microenvironment at the nano scale to regulate cell behavior and function [11]. Recent progress in nanotechnology has revealed new possibility for tissue engineering to design nanotopographic surfaces and nanofeatured scaffolds to provide the closest resemblance to native ECM [12]. Furthermore, it is possible to encapsulate and control the spatiotemporal release of drugs (e.g., growth factors) based on recent developments in drug delivery systems in nanotechnology [12]. This emerging technology can influence cell behavior ranging from attachment to gene expression [12].

Electrospinning is a simple and cost-effective fabrication method for producing a 3D fibrous network, from a wide variety of polymers, in submicron diameters. Accordingly, it has been utilized for producing scaffolds for tissue engineering. The aim of this thesis is to introduce nanostructured fibrous scaffolds fabricated by electrospinning for implantation in tissue engineering. To this end, the relation between the mechanism of fiber formation and morphological variations of electrospun nanofibers is discussed based on key processing parameters in electrospinning. In addition, a novel characterization technique is proposed for precise measurement of structural properties in electrospun scaffolds so as to avoid systematic deviations in characterization of structural properties. Furthermore, a comparative study between the structural properties in nanofibrous scaffold and viability of cells is established to highlight the effects of scaffold architecture in a cell growth. Finally, the attachment, viability, proliferation and differentiation of stem cells in nanostructured fibrous scaffolds fabricated by electrospinning are investigated in order to present the success of implantation of this type of scaffold in tissue regeneration. Therefore, the thesis is presented in four steps, and corresponding to four articles, which are as follows:

In the first step the preparation of nanofiber and nanofiber composites are discussed and the resultant morphologies based on three key elements in electrospinning process (electrical field, surface tension and viscoeleastic behavior of solution) are described. Accordingly, polyacrylonitrile (PAN), carbon nanotube (CNT) and ethylene carbonate were utilized as a precursor polymer, filler and polymer plasticizer respectively.

In the second step, a rigorous technique based on image analysis for the quantification of structural characteristics, and to exploit the results to evaluate the permeation-filtration mechanism are introduced. Our technique enables the computation of layered and overall porosity characteristics of electrospun nanofibres in different morphological conditions. Furthermore, the interconnectivity, scaffold percolative efficiency (SPE), optimal pore size (OPS) and their corresponding relation to depth filtration were studied. The reliability of the proposed approach was validated by measurements and through comparison of the structural characteristics of several samples with different morphological architectures. This section can offer the possibility to evaluate the mechanism of cell infiltration in nanofibrous scaffolds highlighted in step 3.

In the third step, 3D nanofibrous chitosan-polyethylene oxide (PEO) scaffolds were fabricated by electrospinning using different processing parameters. The structural characteristics, such as pore size, overall porosity, pore interconnectivity, and scaffold percolative efficiency (SPE), were observed by a robust image analysis introduced in step 2. To elucidate the correlation between structural characteristics within the depth of the scaffolds' profile and cell viability, a comparative analysis was proposed.

In the fourth step, a new hybrid scaffold constructed by coating electrospun chitosan/polyethylene oxide (PEO) nanofibers on commercial BioTek polystyrene (PS) scaffold obtained from Sigma Aldrich is presented. The characteristics of this scaffold will be compared with commercial BioTek scaffold and TCPS, using some biological analysis including cell viability assay, alkaline phosphatase activity (ALP) and differentiation potential by appropriate methods.

2 NANOSTRUCTURED MATERIALS IN TISSUE ENGINEERING

There are different techniques proposed to exploit cell- nanotopographic interactions to indicate the appropriate cell behavior in engineered tissue (see Figure 1). Top-down lithographic methods such as gratings, pillars, and pits have been used so as to produce various nanopatterns [7]. Methods such as micelle lithography, anodization and electrospinning are employed to produce an array of nanospheres, vertical nanotube and nanofibers respectively [13-15]. Furthermore, polymer demixing, chemical etching, electrospinning, and phase separation processes are used to create less-ordered nanotopographies [16]. In polymer demixing, increased island size resulted to higher interaction of filopodia with the nanotopography of the surface, whereas, no systematic result for proliferation of fibroblast cells in relation to island size was observed.

2.1 Nanotopography and Its Interactions with Cells

Nanotopography of the surface can significantly influence cell morphology, adhesion, proliferation and gene regulation [7]. In general, the most important aspect of utilization of nanotopography in cells function is attributed to the effect associated with cell geometry. As an example, many cells in nanograting processes tend to be elongated and aligned in the direction of the grating axis (see Figure 2) [7, 17]. These cells varied from fibroblasts (size: 50-600nm) to corneal ECs (size: 2–20 μm) [7]. It is noticeable that elongation and alignment of the nucleus may cause to the initiation of secondary effects such as cell signaling and variation in gene profile [7, 18]. Although, the mechanism of such variation unclear and under debate, it is theorized that the origin of such morphological responses can be traced back to the generation of anisotropic stresses [7]. Beyond that, at the molecular level the 3D sharp-tip nanotopographies can influence the formation and rearrangement of intracellular adhesion molecules which subsequently alter other cell behavior such as gene expression and proteins production [19].

In the case of impacts of nanotography on cell proliferation, it was observed that cells on nanogratings exhibit lower proliferation rates than cells cultured on planar substrates. On other hand, the proliferation rate of cells contact with nanopost or nanopit geometries is unpredictable and depends on the substrate material, length scale, cell types and some combination of geometry [7]. It is noted that inability to control nanodimensionality and periodical rearrangements of nano scale surface can be included the possible challenges for systematic assessment of cell function driven by nanofabrication [19]. Chio et al. [19] in their investigation tried to overcome this challenge and structural deviations by controlling in nanodimesionality and nanoperiodically in introduced patterns (nanoposts and nanograte). The results showed that the increased nanotopographical three-dimensionality is accompanied with a reduced number and size of cells. However, cells exhibited a more elongated morphology in three dimensional patterns compared to 2D smooth surfaces. [19]

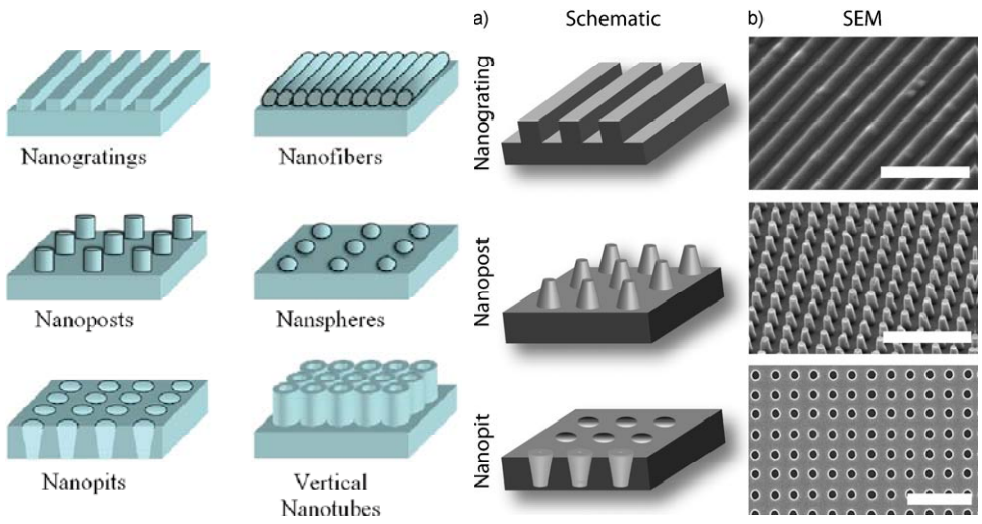

Figure 1. Schematic illustration of nanotopographic fabrication methods [7, 12]

In addition, cell-nanotophography interaction is accompanied by induction of different effects on single cells, resulting from the physicochemical characteristics of the substrate [7]. These may include negative impacts in cells cultivation mechanism such as decreased proliferation in fibroblast cells, mesenchymal, embryonic and endothelial cells [10,17, 20-21] or positive effect such as increased biased migration in corneal ECs and endothelial cells [7,22-23]. It is claimed that cell-nanotopography interactions lead to control of stem-cell differentiation and cellular superstructure which are both beneficial for utilization in tissue engineering.

.

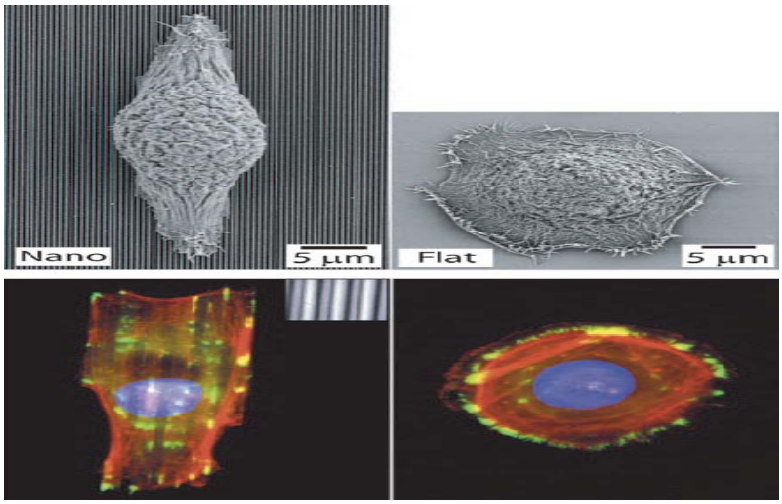

Figure 2. Elongation of epithelial cells along grating axis in nanograting fabrication method [7]

2.2 Electrospun Nanofibers as a Tissue Scaffolds

In tissue regeneration, many attempts have been made to explore the material properties and processing methods offering the highest biomimicry with native tissues. Electrospinning is a straightforward method to produce fine fibers of sub-micron diameter. Recently, the unique properties of electrospun fibers have attracted a great deal of attention for a broad range of applications from particle filtering in membrane science, to cell culturing in tissue engineering [24-27]. In addition to the electrospinning of nanofibers from a pure polymer, it is possible to use this technique for encapsulation of fillers within the nanofiber structure [28-29]. Implantations of 3D fibrous scaffolds can mimic the extracellular matrix (ECM) consisting of proteoglycans [30-31] and the network of protein fibers (50–500nm diameter) [32-36] surrounding the cells in the microenvironment. In particular, a biocompatible nanofibrous membrane fabricated by the electrospinning process has been addressed in many publications as a potential candidate for tissue scaffolds [32, 36-41] and drug carrier mediums [42-45].

Various processing and material parameters have been introduced to control the morphological variations of electrospun nanofibres [46-51]. These variations can be attributed to three crucial factors; the surface tension, charge density, and viscoelastic behaviour of the solution [52-53]. In general, surface tension tends to decrease the surface area per unit mass in fluids, and induces Rayleigh instability to the electrified jet [54-56]. A higher charge density and thus, higher solution conductivity causes a greater bending instability of the driven jet, resulting in a reduction of the fiber diameters [54-55, 57]. Also, variations in the electrical field can influence the mechanism of fibre formation in the electrospinning process [58]. The viscoelastic properties of the solution play a significant role in the dynamics of jet elongation, different instability modes and shape of the Taylor cone [59-62]. However, Yu et al. [62] revealed that the mechanism of fiber formation depends on the elasticity of the polymer solution, rather than its viscosity.

2.3 Structural Characteristics of Nanofibrous Scaffolds and Cells Viability

However, apart from the biocompatibility and mechanical properties, 3D and multilayer architectures as well as the interconnected pore configuration are key structural parameters making the electrospun scaffolds convenient in tissue engineering. Nonetheless, to succeed in exploiting such 3D structural conformations, it is of significance that initially the cells introduced permeate and interact within the different depths of the scaffold profile. In other words, the cellular viability is correlated with the degree of infiltration and attachment of cells within the fibrous matrix. In both in vitro and in vivo systems, regardless of the different aspects in microfluidics of cell intrusion, the cellular diameter and corresponding structural properties have a paramount effect in determining the mechanism of cell culturing. This may be due to the fact that the mechanism of cell growth is a size-dependent phenomenon within the scaffold architecture. For instance, previous literature has reported that, for a successful attachment and permeation of bladder smooth muscle cells, the optimal pore sizes in a scaffold should be around 100–300 μm [63] and for skin regeneration are

20–125 μm [64] while this value for chondrocyte ingrowth is assumed to be between 70 and 120 μm [65]. It is hypothesized that, for cellular size beyond optimal pore sizes, seeded cells with greater size utilize only the surface of the scaffold as an attachment site and might be forming the cellular aggregations based on cell-cell interaction. On the contrary, for cells smaller than optimal diameter, they have a tendency for revisable infiltration (migration) through the depth of scaffold profile (see Figure 3(a)). Both circumstances may reduce cell-matrix interactions, and thus negative trends for cultivation performance could be created. On this basis, the design of the customized scaffold that is able to facilitate the cellular permeation through the depth of a nanofibrous scaffold still remains a challenge in tissue regeneration [66-70]. Beyond this, the small pore sizes prevent vascularization of biomaterials leading to limitations in nutrient delivery and waste removal, resulting in disturbance to the tissue ingrowths [66-67].

To retain inherent processing advantages in electrospinning, it is of the utmost importance that the methods proposed are established based on the fundamental aspects of the fiber formation mechanism in the electrospinning process. In this regard, while processing parameters and solution properties can alter the architecture and morphological characteristics of electrospun nanofibers, it is obvious that they can be utilized as a main or subsidiary technique for the structural modification in an engineered scaffold.

2.4 Chitosan Nanofiberous scaffolds

Chitosan as a biodegradable polysaccharide derived from partial deacetylation of chitin [71-72] has been broadly utilized in the fibrous architecture for tissue scaffolds [73-74] and wound dressings [43, 78]. A chitosan nanofiber scaffold can reduce infection in in vivo implantation due to its antibacterial properties. It offers better cell adhesion, and viability compared to films in hepatocytes cultivation [75]. Apart from nontoxicity and the morphological similarity of chitosan nanofibers to native skin ECM, oxygen permeability, originating from its porosity characteristics, makes it appropriate for wound healing applications [43, 79]. Particularly chitosan will gradually depolymerize in to *N*-acetyl-d-glucosamine enables it to initiate fibroblast proliferation, and associates in ordered collagen deposition and stimulates the increased degree of natural hyaluronic acid synthesis in the wounded regions [43, 79-80].

Pure chitosan is difficult to electrospin, and the mechanism of fiber formation can be facilitated by blending with cospinning polymers. The cospinning polymers can lead to higher chain entanglement, which is a main prerequisite in electrospinning for attaining nanofibers with fewer structural imperfections [81]. In addition, the mixing of chitosan with other polymers may result in a closer analogy of the scaffold to natural ECM components or offer superior properties in tissue regeneration. Fibrous chitosan composites produced by electrospinning have been widely reported in previous publications [42, 73, 76, 77, 81-86]. For instance, chitosan/PEO nanofibers can be utilized as a three dimensional scaffold for cartilage tissue repair due its good adhesion, proliferation, and viability for chondrocytes [86]. The strong hydrogen bonding in chitosan and PEO chains leads to polymer blends being electrospinnable [87] (see Figure 3(b)).

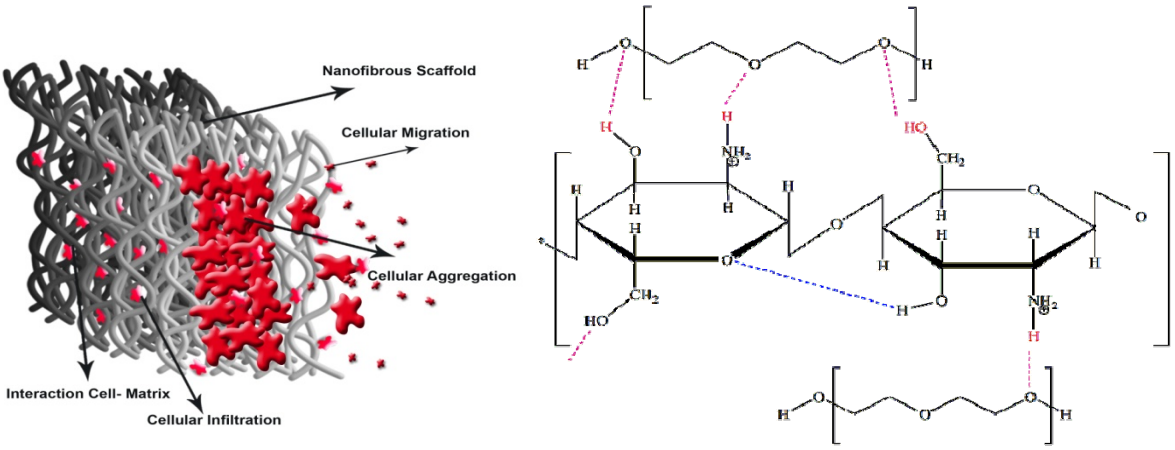

Figure 3: (a) Schematic illustration of interactions between cells and nanofibrous scaffold (matrix). (b) Chemical structure of chitosan/PEO polymer chains and their hydrogen bonding.

2.5 Simulation of Structural properties of Nanofibrous Scaffolds

The structural properties of electrospun nanofibers originate mostly from the random deposition of ultrafine fibres in the form of an interconnected porous substrate, resulting in a rapid increase in filtration accompanied by reduced permeability loss [88-91]. Characterization of these parameters could pave the way to estimating the relative implantation efficiency of the membranes in demanding applications where the quality of depth filtration is paramount. Lithium battery membranes [92-93], tissue scaffolds [94-95], and separation membranes for fuel cells [96-97] are the most common applications for electrospun membranes for depth filtration.

A review of the related literature revealed that there is no satisfactory correlation between structural characteristics and the permeation-filtration process throughout the depth of a membrane. Exploring the interplay between depth filtration behaviour and structural characteristics expedites the process optimization of electrospinning parameters to produce ideal membranes for demanding applications. The proposed approach involves the evaluation of these properties without the use of the complex theoretical equations typically attributed to depth filtration dynamics, the majority of which have no correlation with processing parameters.

Image analysis is a non-destructive characterization method and, due to its ability to detect individual pores, is beneficial for structural characterizations. The most important advantage of image analysis, particularly with respect to the unique architecture of nanofibres, is the ability to conduct porosity measurements within the depth profile of the image. However, in order to exploit accurate results of quantitative analysis, careful consideration should be paid to morphological

features either by means of programming or software implementation. Consequently, previously proposed algorithms [98-101] are appropriate only in specific cases, and general process conditions still present key obstacles regarding their effectiveness. These obstacles mainly originate from structural imperfections (beading and solution dripping) and high or low density of fiber deposition. Such measurement obstacles, especially at the nano scale, hinder the precise evaluation of the actual elements involved in depth filtration.

2.6 Nanofibrous Scaffolds and Stem Cells

Stem cells provide vital properties required for certain tissue engineering applications. For instance, the number of cells required by using primary tissue maybe considered as part of a challenge for certain tissue therapies, while stem cells as a alternative solution enable to reproduce the cells by ability to differentiate in specific lineage. In addition, decreased immunogenicity and potentially immunosuppressive characteristics have been made the stem cell as an appropriate source of cells for regenerative medicine. [102-104] In general, stem cell fate is attributed to genetic and molecular mediators such as growth and transcription factors. However, the new surveys have been developed the idea that the influence of solid state environment, such as interaction of ECM ligands with cell surface receptors, is significant in control of cells behavior. However, the ECM-based control of cells may lead to multiple physical mechanisms such as ECM micro and nano structural properties, ECM elasticity or mechanical signals transmitted from the ECM to the cells. [105] As an example, it is possible to manipulate the human mesenchymal stem cell (hMCS) fate by altering the dimensions of nanotubular titanium oxide. This is due to small nanotubes sizes increased the cellular adhesions whereas the larger sizes led to elongation of stem cells resulting in induce cytoskeletal stress and obsteogenic differentiation. Mesenchymal stem cells (MSCs) are multipotential stromal cells able to differentiate into a wide variety of cells, e.g. bone, cartilage, fat, muscle, marrow stroma and other tissue types, when they are exposed to appropriate biological cues [106-107]. Hematopoietic and non-hematopoietic cells are considered to be the source of MSCs and are found in bone marrow [106, 108]. Human mesenchymal stem cells (hMSCs) can differentiate into different lineages including osteoblasts, adipocytes, and chondrocytes (in the form of high-density cell pellets) [109]. The availability of a single 3D scaffold enables the maintenance of biological cues for mesenchymal stem cells to differentiate into more than one lineage, which is of particular interest in regenerative medicine. In general, cell attachment, proliferation and osteogenic differentiation of MSC are promoted by utilization of nanofiber scaffolds [110-111]. Nanotopography, ECM structural resemblance and chemical composition of nanofibrous scaffold can enhance the potential of osteogenic differentiation [105, 110, 112]. However, this trend can be further promoted by biomimetic modification of nanofibers, e.g. by inclusion of exogenous growth factors [105, 111, 113]. Several previous studies have noted the commitment of MSCs to osteogenic differentiation in nano-fibrous scaffolds [102-105, 110], whereas only a few have addressed their potential for the adipocyte lineage [109, 114]. In general, the dedication of MSC to a specific lineage is caused by different cues in the microenvironment [115]. These cues, in addition to

structural analogies of scaffold to native ECM, may involve other distinct parameters such as cell shape, cytoskeletal tension, RhoA, scaffold orientation and elasticity or even secretion of soluble growth factors into the culture medium [115-117].

As mentioned before, ECM plays an important role in tissue regeneration due to its modulating impacts on the adherence, viability, proliferation, differentiation and self- renewal of stem cell [118]. In addition to biophysical and biochemical analogies, introducing a scaffold with the highest structural similarity to ECM can provide better compliance with stem cell behavior. Many investigations have been conducted for the preparation and characterization of three dimensional scaffolds fulfilling the required architecture of ECM in micro-environments [119-124]. However, constructing a customized scaffold having structural mimicry with the architectures and topographies of ECM still poses some challenges. These obstacles may originate from the complex structure of ECMs constituted from protein nanofiber networks forming a micro-porous structure in three dimensional status. This structural complexity may also increase the interaction of ECM-cells, leading to high cellular intrusion, nutrient and oxygen permeation, waste removal and vascularisation in tissue regeneration [119]. Therefore, some significant structural criteria such as micro-porosity, pore interconnection and nano-scale fibers should be considered in the modeling of customized scaffolds. Electrospinning is a simple and cost-effective fabrication method for producing a 3D fibrous network, from a wide variety of polymers, in submicron diameters. Accordingly, it has been utilized for producing the scaffold for tissue engineering. Although electrospun fibrous scaffolds have many structural resemblances to ECM, their packed morphology and nano-scale pore size limit the mass transfer necessary for tissue regeneration [124-127]. In order to tackle this problem, various approaches have been proposed for increasing fiber diameter and subsequently pore size. However, the results of these techniques have not been completely satisfactory [127-130].

It has been noted that implantation of hybrid micro/nano scaffolds with combined characteristics of micro-porosity and nano-scale fibers appears to be a successful strategy for constructing native ECM analogies.

3 MATERIALS AND METHODS

In this chapter, all of materials used in this thesis and the methods that were implemented, (such as electrospinning, structural characteristics simulation, cells cultivation and biological tests) are explained in detail.

3.1 Materials

Polyacrylonitrile (PAN) was used at different concentrations as the polymer component for creating solutions with varying viscosities. The viscosity of PAN at 10 wt% concentration was 0.3 Pa.s at room temperature. N, N-Dimethylformamide (DMF) was purchased from Baker. Multi-wall carbon nanotubes (MWCNT) with an average diameter of 9.5 nm, an average length of 1.5 μm, and a carbon purity of 90%, produced via the catalytic chemical vapour deposition (CCVD) process, were purchased from Nanocyl. Ethylene carbonate (C3H4O3) was purchased from Merck Chemicals. Low molecular weight chitosan (M_W = 120 kD_a) with a degree of deacetylation (DD = 75–85%) was purchased from Fluka, Switzerland. Polyethylene oxide (M_W = 900 kD_a) was purchased from Sigma Aldrich, USA. Both glutaraldehyde solution (GA) 25 wt% in H_2O and acetic acid (glacial) 100% were obtained from Merck Co., Germany. 3D Biotek 3D Insert™ PS scaffold (96 well compatible, fiber diameter 150μm, pore size 200μm, 24 inserts/pack) was purchased from Sigma Aldrich, USA. Mouse connective tissue fibroblast cells (L929) were obtained from the Pasteur Institute of Iran (NCBI), cultured in RPMI 1640, and maintained in an incubator with a humidified atmosphere of 5% CO_2 at a temperature of 37°C. RPMI 1640 and trypsin were purchased from local vendors, originally made by PAA (Austria). Human Mesenchymal stem cells (hMSCs) were obtained from Stem cell technology research center, Tehran, Iran. Other reagents were obtained from Sigma Aldrich, USA unless stated otherwise.

3.2 Electrospinning

3.2.1 Electrospining of PAN nanofibers and PAN/CNT nanocomposite fibers

Plain polymer solutions were prepared by dissolving PAN in DMF and a magnetic-mechanical mixer stirred the solutions for 2 hours at 80°C. In order to prepare the PAN/ CNT nanocomposite fibre, CNT was added to the DMF solvent and sonicated for 30 min to obtain an homogenous solution. Subsequently, in some samples, EC with a different weight fraction was added to the CNT/DMF solutions in order to study the effects of EC on the morphology of an electrospun web (see Table 1). Similarly, PAN was dissolved in the CNT/DMF solutions and stirred for 2 hours at 80°C by a magnetic mechanical mixer. The nanofibres were spun by a one-nozzle electrospinning system perpendicularly aligned to the target collector. The electrospinning system consisted of; a high voltage source (bipolar Simco Charge master BP 50), a nozzle (a glass vessel containing the polymer solution and a metallic needle), and a copper collector electrode plate. The applied voltage

was generated by connecting the nozzle and the collector plate to the positive and negative terminals of the high voltage supply, respectively. The voltage difference between the needle and the collector was set at 40 kV (nozzle +20 kV and plate -20 kV) with a needle tip-to-collector distance of 15 cm. A metallic needle (14G) with an inner diameter of 1.6 mm, and a length of 10 mm was used for ejecting the polymer solutions towards the collector. The collector plate was covered with paper to gather the resultant fibers at a specified distance.

Table 1. The solutions composition and their correspondent viscosity

Trial code	PAN wt%	CNT wt%	EC wt%	Viscosity (Pa.s)
	6	0	0	0.1
	8	0	0	0.2
A	10	0	0	0.3
	12	0	0	0.7
	14	0	0	1.5
	10	0.25	0	1.2
	10	0.5	0	51.9
B	10	0.75	0	68.6
	12	0.5	0	53.7
	10	0.25	1	1.2
	10	0.25	2	1.2
C	10	0.25	4	1.2
	10	0.25	6	1.2

3.2.2 Electrospining of Chitosan/ PEO nanofibers

PEO was used as a cospinning component in the chitosan solution due to the difficulty of forming the continuous fibers without structural imperfections from neat chitosan in the electrospinning. Both chitosan and PEO were prepared at 2.5wt% and dissolved solely in 90 Vol% acetic acid. Subsequently, chitosan and PEO solution in a weight fraction of 90: 10 were mixed and stirred by mechanical mixture for 24 hours so as to make the solution homogenous. The nozzle syringe was loaded with 5mL of chitosan/PEO solution and the rest of the confined air in the syringe was evacuated completely. A metal capillary (needle of gauge 18, inner diameter = 0.84 mm) was inserted at the tip of nozzle. The electrospinning was performed by fully automated Electroris (Fananvaran Nano-Meghyas) equipment. The collector was covered in aluminum foil, and the anode and cathode electrodes were connected to the collector and the tip of metal capillary, respectively. Subsequently, feed rates, tip to collector distances, applied voltages, and constant rate of traverse were set by the control panel of system. Finally, the chitosan/PEO solution was electrospun based on the different processing parameters summarized in Table 2. Each sample was electrospun on the condition that only one processing parameter was changed while other parameters remained constant. To prevent the dissolution of the chitosan scaffolds in the culture medium, as well as to provide a control on chemical and water solubility, they were cross-linked

under exposure of vaporized glutaraldehyde (GA), rising from 5mL GA solution in a desiccator, at room temperature for 48 hours.

Table2. A summary of electrospinning setup and the corresponding processing parameters for each sample scaffold.

Sample Code		Deposition Time (h)	Feed Rate (ml.h^{-1})	Applied Voltage (kv)	Distance(cm)
Variation on Time	1	1	0.27	8	13
	2	2	0.27	8	13
	3*	3	0.27	8	13
	4	4	0.27	8	13
Variation on Feed Rate	5	3	0.17	8	13
	6	3	0.37	8	13
Variation on Voltage	7	3	0.27	10	13
	8	3	0.27	13	13
	9	3	0.27	15	13
Variation on Distance	10	3	0.27	8	10
	11	3	0.27	8	15

*Control sample was electrospun with constant processing parameters; deposition time=3 h, Feed rate= 0.27 ml.h^{-1}, applied voltage= 8 Kv and tip to collector distance= 13 cm

3.2.3 Fabrication of Micro/Nanostructured Hybrid Scaffolds

Chitosan/PEO solution in 90:10 wt% was prepared as described previously in Part 3.2.2. PEO was used as a co-spinning reagent in the electrospinning of chitosan so as to produce nanofibers without structural imperfections. The electrospinning process was performed in fully automated Electroris (Fanavaran Nano-Meghyas, Iran) equipment. The collector was covered by aluminum foil and then the commercial BioTek PS scaffolds were placed on the collector. A metal capillary (18 gauge needle, inner diameter = 0.84 mm) was inserted at the tip of the nozzle. The anode electrode was connected to the collector while the cathode was attached to the tip of the metal capillary. The electrospinning processing parameters, including applied voltage, nozzle to collector distance, feed rate and deposition time, were set by the control panel of system to 10 kV, 13 cm, 0.35 mL/h and 300 sec, respectively.

3.3 Characterization of Electrospun Nanofibers and Scaffolds

In this section, the methods used for characterization of electrospun nanofibers and scaffold are described in detail. The characterization methods were including, morphological observation SEM images), viscometery, electrical conductivity, structural characteristics obsevation and biological tests.

3.3.1 Morphological Observation

The morphology and fiber diameter of the electrospun nanofibres were observed by Zeiss Ultra Plus SEM and FE-SEM, Hitachi S4160 equipments. To take an SEM image of the nanofibre pattern, the samples were coated in gold to make them conductive. Image J software version 1.43a was used for measuring the fiber diameter from the SEM micrographs. The mean fiber diameters were calculated from 100 measurements of each sample.

3.3.2. Viscometery and Electrical Conductivity Measurements

Viscosity was measured with a Brookfield DV-II+ viscometer at room temperature. The mean electrical resistance of PAN solutions with different CNTs and EC loads at 10 wt% was measured. The mean solution conductivity was evaluated through resistance, the reciprocal of the conductance, by five measurements with an ohmmeter.

3.3.3 Structural Characteristics Simulation by Image Analysis

The permeability and filtration properties of a fibrous membrane were determined as a function of three crucial parameters, known as the open area, solid area and interconnection. The proposed method relies on the projection of the open area (overall porosity) and solid area (fibrous network) from the image in the 2D plane. While the interconnection is estimated by the trend of blocking pore channels throughout the depth of the membrane profile [98]. This trend can be identified as an increase in cumulative open area from sublayers to the surface layers at the membrane profile (see Figure 4).

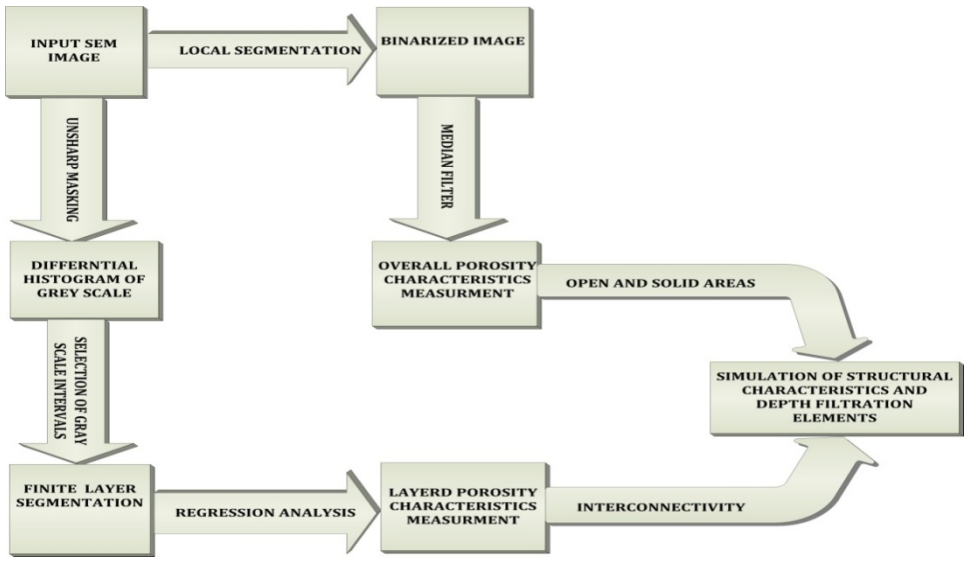

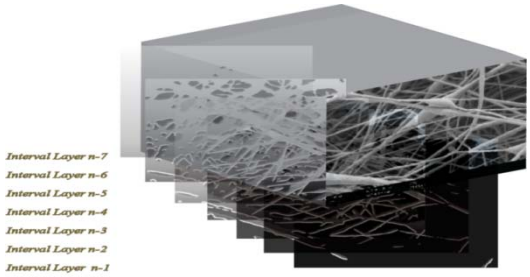

Figure 4. a) Flow chart of the proposed image analysis method, b) 3D illustration of electrospun membrane segmented by seven cumulative layers (interval layers) from infinite n layers

3.3.3.1 Segmentation Procedure

The first step of the proposed algorithm involves precise segmentation of a 256 grey-scale image to binary form using the threshold procedure. Thresholding is a simple but effective process for object segmentation from the image background. The procedure is also essential with regard to obtaining measurement accuracy, and the selections of the following sequences of morphological operations are highly depending on it. Among the aforementioned thresholding methods, only local thresholding seems to meet the structural requirements of a fibrous membrane. This may be due to the multilayered architecture of the membrane, since the intensity gradient of the image is inhomogeneous, varying locally from surface to sublayers. The non-uniform intensity gradient throughout the membrane profile prevents realistic binarization. The local criterion approach can tackle this segmentation problem by dividing the image into various subimages. The boundaries of local sub-images are determined based on neighbouring pixels within a specific radius, while the threshold values dynamically change over these boundaries [131-135].

In addition, based on the local approach, deviations caused by applying different magnifications are minimized by selecting the radius of the local region proportionally to the change in magnification. Several local thresholding methods have been developed, the most commonly applied of which include mean, median, MidGrey, Bernsen, Niblack and Sauvola [131,136]. Among these methods, Bernsen and Sauvola (as an improved version of Niblack) have inherent advantages for use in high contrast areas. However, Sauvola thresholding is edge-sensitive and more appropriate for high-contrast regions with some faint connection [131,137-139]. On this basis, the Sauvola method seems to be particularly suitable for fibrous membranes where fibers intersect on several layers forming a porous architecture. Experimental observation of nanofiber images confirmed this theoretical concept. As shown in Figure 5, the Sauvola method exhibits structural imperfections (beads, solution dripping) and fiber deposition more realistically than other versions. The local threshold $T(i,j)$ is indicated as a function of the coordinates (i,j) at each pixel calculated from Equation (1) [131]:

$$T(i,j) = m(i,j) + \left\{ 1 + K \left[\frac{\sigma(i,j)}{R} - 1 \right] \right\} \quad (1)$$

where k=0.5 and R=128 (k and R are constant)

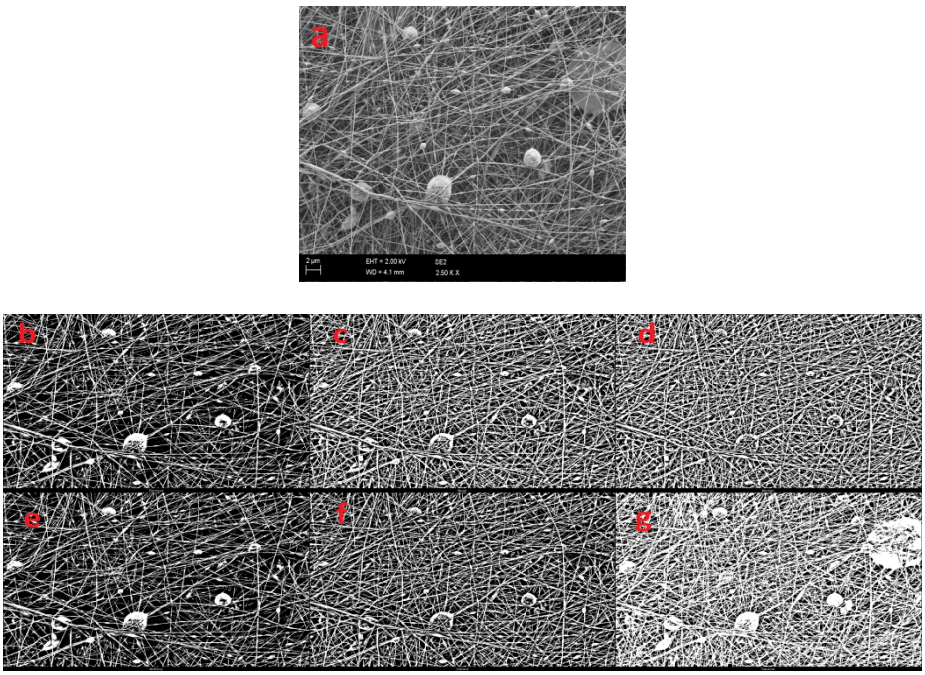

Figure 5. Original and binarized images by different local thresholding methods at radius r=15, a) Original SEM image (magnification 2.5 KX), b) Bernsen, c) Mean, d) Median, e) MidGrey, f) Niblack, g) Sauvola

3.3.3.2 Porosity Characteristics Measurement

Depending on the preferred accuracy of measurement, m number of images are selected and converted to binarized mode and the mean porosity computed from Equation (2) [98]:

$$\bar{P} = \sum_{i=1}^{m} P_i = \frac{1}{m} \sum_{i=1}^{m} \sum_{j=1}^{n} \frac{a_{ij}}{A} = \frac{1}{mA} \sum_{i=1}^{m} \sum_{j=1}^{n} a_{ij} \quad (2)$$

where A is the total scanned area, *aij* is the pore area *j* found on the image *i* of the corresponding nanofibre mat. *Pi* is the porosity calculated based on the image number (*i*) and *m* is the preferred number of images. To reduce image noise and irregular clustering of pixels, applying a median filter as a smoothing morphological operator and defining a minimum cut-off value for recognizing

the interested areas is highly recommended. The size (radius) of local windows for the median filter should be proportionate to the relative ratio of magnification. The pore size was evaluated by measurement of the maximum Feret's diameter, which is defined as the longest distance between two parallel tangents at an arbitrary angle in the boundary of a pore area [140-142].

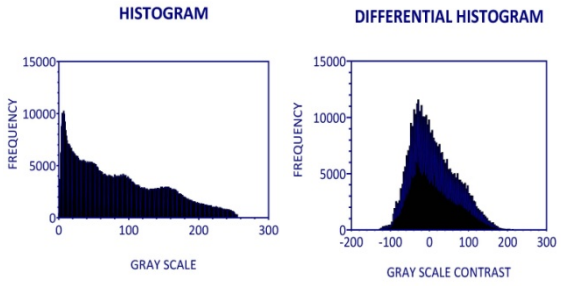

Figure 6. Comparison between a) a grey-scale histogram and b) a differential histogram of grey-scale contrast after unsharp masking

3.3.3.3 Layered Porosity Characteristics Measurement

To study the depth filtration behaviour based on solid and open area, the structural elements throughout the profile need to be accurately measured layer by layer. Finding the edge of overlapping layers by analysing the intensity variation at selected local windows seems to be the best approach for layer-by-layer segmentation. One practical method is to use a differential histogram of intensities by applying unsharp masking where the edges of overlapped fibers are more discriminated. Unsharp masking is a manipulating technique used in image processing that achieves edge enhancement by amplifying components with the high intensity [143-145].

In the algorithm, a median filter, which is well-known to remove local outliers from images [146-147], is used as the unsharp operator at the selected local window. After unsharp masking, the histogram of grey-scale contrast has a unique feature that can be used to locally segment the edge of objects from the background. This approach is well-suited for our purposes because the image edges (high intensity contrast) are positioned exactly at the layer interface. By exhibiting local contrast values, the differential grey-scale histogram provides important statistical parameters for layer-by-layer segmentation (see Figure 6(b)). Theoretically, if we consider the differential histogram as a curve, the area bounded by *x*-*y* (grey-scale contrast-frequency) plane represents the total pixels in the image. By selecting a specific grey-scale interval, the number of pixels within a distinct grey-scale level can be calculated. The result obtained from this integral calculation is the solid area (fibrous network) in a given grey-scale interval. Subtracting this solid area from the total area gives the layered pore area between two points (c and d) of grey-scale contrast. Furthermore, the layered porosity fraction at [c,d] can be calculated from Equation (3):

$$P_{cd} = 1 - \frac{\int_c^d t(x)dx}{\int_a^b t(x)dx} \qquad d > c \tag{3}$$

where t (x) is the differential histogram curve, b and a are respective supremum and infimum of greyscale contrast, and P_{cd} is the layered porosity fraction at the [c,d] intensity interval. This approach has good compatibility with random deposition of fibre in an electrospinning mechanism in which each nanofibre layer is positioned at different depths throughout the membrane profile and should be identified by a specific interval rather than a discrete value for grey-scale contrast. By extracting statistical data such as mean (μ) and standard deviation (σ) from the differential histogram, it is possible to select the best intervals (INT) that precisely simulate a fibrous network with finite layers. To add the interconnectivity of the layers to simulation, the interval sequence should be such that each interval overlaps with the previous one, with the last interval covering the entire range of grey-scale contrast (Equation (4)):

$$INT_n=\{\forall x, x, n \in N_0 \ , x \leq n : L_x = [\mu \pm x\,\sigma, b]\} \cup \{[\sigma, \mu], [a, b]\},$$
$$L_x \subset [a, b] \quad (4)$$

The number of intervals needed for layered simulation depends on the statistical parameters of standard deviation, mean, supremum and infimum of grey-scale contrast. The slight reduction in pore area due to overlapping of different layers in the fibrous network can be shown by defining the discrete function R_x exhibited in Equation (5) [98]:

$$R_x = \left(\sum_{i=0}^{n} a_i / A_T\right)_x \quad (5)$$

where x is the number of layers, a_i is the remaining pore area after x layer depositions, and A_T is the total area. Overlapping of several layers causes narrowing of the open areas until the penetration channel is totally blocked. If Equation (5) is substituted by data from the greyscale contrast, from the modelling using a (infimum value) as the sublayer and b (supremum value) as the surface layer, the equation exhibits an increasing trend. This equation can be modified in the form of Equation (6):

$$R_x = 100 \times \left(1 - \frac{\int_x^b t(x)dx}{\int_a^b t(x)\ dx}\right) \qquad x \leq b \quad (6)$$

From Equations (3) and (6), when $x = c$ and $b = d$, it can be concluded that the numerical value of blocking open area is equivalent to the layered porosity at depth x in the membrane ($R_x = P_{xb}$).

Based on the above data, the interconnectivity of the fibrous membrane can be estimated by finding the best fitted curve (trend) derived from regression analysis of layered porosities throughout the depth of the membrane. Based on the bell shape of grey-scale contrast histogram and related mathematical principles, it was found that dose-response curve is the best model for evaluating the best trends for layered porosities in our simulation (see Figure 7). Dose-response curves are generally used to explain the results of in vitro experiments where the known concentrations of a drug are varied. This template can be extended to any experiment where corresponding results are

compatible with the basic principle of dose-response relations through variation of a known parameter.
In the present study, however, the aim was to apply this model to layered porosity only with respect to regression of results based on mathematical features, as opposed to dealing with dose-response relations. The following two aspects of dose-response regression [148] are of key importance to our simulation:

1) Half way open area (O_{50}): the cumulative layer with a half open area in the membrane
2) Hill slope (H): the steepness of dose-response curve is described by the hill slope, where a higher value indicates faster blocking of accessible channels (less interconnectivity), and a low value indicates that the open area narrows moderately (high interconnectivity).
On this basis, H can be assumed to be the reciprocal index of interconnectivity of the membrane. The general model for best fitted curve for layered porosities is illustrated in Equation (7):

$$F(x) = \frac{100}{1 + 10^{((O_{50} - x) \times H)}} \tag{7}$$

where O_{50} is the half way open area, x is the grey-scale contrast and H is the hill slope of the dose-response curve.

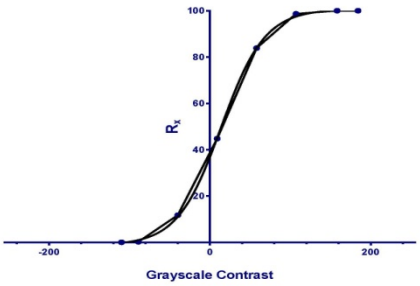

Figure 7. Best-fit (dose–response) curve for layered porosity from non-linear regression analysis

3.3.3.4 Intrinsic structural properties and their relation to depth filtration elements

Tehrani *et al*. [98] introduced a factor known as scaffold percolative efficiency (SPE) to contribute interconnectivity and mean porosity to characterization of permeation properties of an electrospun membrane. They hypothesized that an exponential curve is the best fit for layered porosity regression, and its slope (b) can be assumed as a reciprocal index of interconnectivity. However, the layered porosity measurement via our algorithm revealed that the exponential curve was not

sufficiently compatible for exhibiting the layered porosity trend. Therefore, the scaffold percolative efficiency factor (or permeation efficiency constant) was modified via our approach as follows:

$$SPE = \frac{P}{b} \xrightarrow{Modified} SPE = \frac{P}{H} \quad (8)$$

where *P* is the overall porosity, *b* is the slope of the exponential curve and *H* is the slope of the best-fit curve. In depth filtration, regardless of theoretical and empirical expressions attributed to dynamics and size of particles, the fractural permeation and filtration efficiency are correlated to porosity and solid area fraction (fibrous network). The fractural filtration efficiency is measured by Equation (9) [149]:

$$E(d_p) = 100 \times \left(1 - \frac{C_2(d_p)}{C_1(d_p)}\right) \quad (9)$$

where $C_1(d_p)$ is the upstream and $C_2(d_p)$ the downstream concentration corresponding to particle size d_p. If it is assumed that each cumulative layer acts as a discrete filtration element based on its pores size and solid area (fibre network), $E(dx)$, as filtration efficiency of the layer positioned at point x in the depth profile can be determined from Equation (10):

$$E(dx) = 100 \times \left(1 - \frac{C_2(d_p)}{C_1(d_p)}\right) = 100 \times \left(-\frac{dC}{C}\right) \quad (10)$$

During depth filtration, the rate of change in particle concentration passing through the depth profile is proportional to the concentration and constant filtration efficiency of the membrane (α) [150].

$$\frac{dC}{C} = -\alpha\, dx \quad (11)$$

In the grey-scale contrast histogram, $\alpha\, dx$ represents the interval (area) in which the permeated particles are filtered at depth x in the membrane profile. This area, known as solid area fraction, is determined by the fraction of fibrous networks at depth x in membrane profile (Equation.12):

$$-\alpha\, dx = \frac{\int_x^b t(x)dx}{\int_a^b t(x)\, dx} \quad (12)$$

From Equation (6) and (12), it can be concluded that:

$$\alpha\, dx = \frac{R_x}{100} - 1 \quad (13)$$

$$E(dx) = 100 - R_x \quad (14)$$

The overall filtration performance of the membrane can be measured from Equation (15) [151-152], where E and P are the filtration and permeation in the membrane.

$$E = 100 - P \qquad (15)$$

As represented in Equation (14-15), it can be concluded that the permeation efficiency follows an identical trend to F(x) (layered porosities approximation), along with adherence to the negative trend of filtration efficiency in the depth profile of the membrane.
For optimization of the membrane for depth filtration, the permeation and filtration efficiency should be identical to 50% (x= O_{50}, F(x) = 50%). Computing the pore size distribution at this point may facilitate the elucidation of quality of depth filtration for particles within a specific geometrical range. Furthermore, the quality of depth filtration is dependent upon the range of pore size within the membrane. This range can be named as the optimal pore size (OPS) and can be estimated based on mean pore size of the total and half open areas, and directly correlates to the size of open areas within the interconnected structure.

As mentioned earlier, overall porosity and SPE are estimated based on averages of n arbitrary images captured from several regions within the membrane. However, in the case of depth filtration elements such as F(x) and OPS, due to inhomogeneous distributions of fibres throughout the membrane, the comparison should be done on a regional rather than overall basis. As an example, the reciprocal interconnectivity index and OPS of two images from different membranes shown in Figure 5 are measured and reported as follows: OPS_1= [212-482], H_1= 0.03, OPS_2= [370-530] and H_2=0.02. As shown in Figure 8, the trace of simulated halfway open channel (E=P, F(x) = 50%) can be identified more readily in the projection of total open area (overall porosity) in membrane 2 compared to membrane 1. This is due to higher interconnectivity and lower tendency for blocking accessible channels of membrane 2. It is noticeable that the OPS parameter is only a comparative index for scaling the interconnected open area that is capable of hosting the transport media in the 3D architecture, but cannot reflect the real optimal particle distribution without consideration of transport media dynamics in depth filtration.

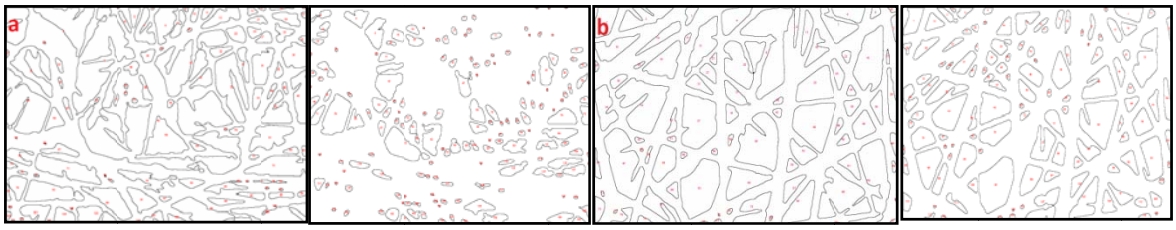

Figure 8. Comparison between simulated open pore areas of a) the sample image with $F(x)_a = \frac{100}{1+10^{((3.31-x)\times 0.03)}}$ and b) the sample image with $F(x)_b = \frac{100}{1+10^{((2.66-x)\times 0.02)}}$ at the half cumulative layer (x= O_{50}) and the projection of open area in the 2D plane (overall porosity)

3.3.3.5 Method implementation and validation

The overall porosity, mean pore size, interconnectivity and SPE of each membrane were characterized based on four FESEM images captured from different areas of the electrospun web. The proposed algorithm was implemented by ImageJ (version 1.43m), a common-use scientific Java-based software [153], in order to increase its usefulness in real-time applications. To investigate and affirm the reliability of non-linear approximation of layered porosities, the GraphPad Prism [154] commercial and scientific software was used. The results were discussed and validated based on empirical observations of perfect nanofibre membrane structures. In the case of depth filtration elements such as F(x) and OPS, the measurement and comparison were done on a regional basis. Mean fibre diameters were evaluated based on 40 measurements of each sample membrane.

3.3.4 Biological Characterizations

Some biological analysis including cell viability assay, alkaline phosphatase activity (ALP) and differentiation potential by appropriate methods are presented in this section.

3.3.4.1 L929 Cells Viability (MTT Assay)

L929 cells were cultured in RPMI 1640 medium supplemented with 10% fetal bovine serum (FBS, Gibco, Scotland) and maintained at 37˚C in a humidified atmosphere with 5% CO_2. When the cells reached >80% confluency, they were detached using 1 ml of 0.25% trypsin as mentioned previously [50]. Each sample scaffold was cut according to the diameter of the wells and each scaffold was placed into a separate well from a sterile 96-well tissue-culture polystyrene plate. Each well was seeded with 200 µl of the cell suspension (10^5cells/ml). Empty wells were used as a control for cell attachment for a sample of the scaffold. The samples were sterilized under exposure to UV for one hour. *L929* cells were allowed to proliferate for 48 hours in the presence of chitosan/ PEO scaffolds and were then rinsed with 200 μL/well phosphate buffer (PBS) to remove the unattached cells before adding MTT (5mg/mL of PBS, Merck, Germany). The MTT assay is a quantitative colorimetric method based on reduction of the yellow tetrazolium dye (MTT) to purple insoluble formazan through mitochondrial succinic dehydrogenase. This method enables the evaluation of metabolically active cells, which directly reflects the cells viability. To this end, a mixture of serum free culture medium and MTT solution in fraction of 30:70 was added to each well. The MTT assay was performed as mentioned previously [155]. The MTT assay was repeated for each sample scaffold three times ($n = 3$).

3.3.4.2 MSCs Viability (MTT Assay)

In vitro cytotoxicity experiments were evaluated using 3-[4, 5-dimethylthiazol-2-yl]-2, 5-diphenyltetrazolium bromide (MTT) assay. MSCs were seeded in 96-well plates at a density of 2000 cells/100µl/well and incubated at 37º C in an incubator with an atmosphere of 5 % CO_2 with

95 % relative humidity for 6 days. On days 2, 4 and 6, MTT solution (Sigma) was added to the plates and incubated for another 3 h at 37 ºC. Then, the medium was removed and 100µl DMSO was added to each well. The plates were shaken slowly and pipetted to dissolve the dark blue formazan crystals generated by the live cells before color intensity was measured. The absorbance of each well solution was measured by a microplate reader (BioTek, USA) at a wavelength of 570 nm. All the experiments were carried out in triplicate.

3.3.4.3 DAPI Staining

To verify the presence of cell adhesion on scaffolds, 4′, 6-diamidino-2-phenylindole (DAPI) staining was carried out. In brief, the scaffolds were three times washed with PBS and the attached cells were fixed with 4% paraformaldehyde for 10 minutes. The scaffolds were then three times washed with PBS for 5 minutes. 1 µg/ml DAPI (Sigma) was added onto the scaffolds and incubated for 5 minutes. Fluorescent images were recorded by Nikon TE2000 microscope (USA).

3.3.4.4 In Vitro Differentiation into Osteoblasts and Adipocytes

For differentiation into osteoblasts, MSCs were plated for 21 days at a concentration of 6,000 cells/cm^2 in 24-well plates and incubated with DMEM (Invitrogen) supplemented with 10 mMβ-glycerol phosphate, 50µM ascorbic acid-2 phosphate (Sigma) and 10^{-7} M dexamethasone (Sigma). For Alizarin red staining, the cells were fixed for 5 min with 70% ethanol at 4°C to determine calcium deposition. To induce differentiation into adipocytes, The cells were plated at 1,000 cells/cm^2 in 24-well plates in DMEM with 1 µM dexamethasone, 10 µg/ml insulin, 0.5 mM IBMX (Sigma) and 100 µM indomethacin (Sigma). After 2 weeks, the cells were fixed in 5% Paraformaldehyde (Sigma) for 30 min and incubated with Oil Red-O (Sigma) to stain lipid vacuoles.

3.3.4.5 Alkaline Phosphatase Activity

ALP activity was measured by total protein extraction of differentiated cells using 200 µl RIPA lysis buffer. For sedimentation of cell debris, the lysate was centrifuged at 6000 RPM at 4 °C for 15 min. Then, the supernatant was collected and ALP activity was measured using Alkaline Phosphatase Activity Colorimetric Assay Kit (Biovision). The optical density of samples was measured at 405 nm in a micro-plate reader (BioTek).

3.3.4.6 Calcium Content Assay

The amount of deposited calcium was measured using Cresolphthalein Complexone method. To extract calcium, the differentiated cells were homogenized in 0.6 N HCl (Merck) followed by shaking for 4 h at 4 °C. After addition of reagents (Calcium Content Kit, Pars Azmoon), optical density of samples was measured at 570 nm in a micro-plate reader (BioTek). Calcium content

values of the samples were obtained from a standard curve of OD versus a serial dilution of calcium concentrations.

3.3.4.7 Quantitative RT-PCR

Relative quantification of osteoblastic specific genes, including Runt-related transcription factor 2 (Runx2), osteocalcin (BGLAP), osteonectin and adipocyte specific genes as well as PPARG and UCP1 of differentiated cells, was carried out on MNHS and commercial PS scaffold compared to control. Total RNA was extracted using QIAzol (QIAGEN). Revert Aid First Strand cDNA synthesis kit (Fermentas) was used to synthesize complementary strands. Real-time RT-PCR was performed using SYBR Premix Ex Taq (TaKaRa Bio Inc.). PCR parameters included denaturation at 95 °C for 30 s, then 40 cycles at 95 °C for 5 s, and annealing/elongation at 60 °C for 30 s. The relative quantification model was applied to calculate the expression of target genes in comparison to HPRT1 used as endogenous control. Gene expression levels were quantified by a Rotor Gene 6000 instrument (Corbett). Primer sequences are illustrated in Table 3.

Table 3. Primers used in real-time RT-PCR

Gene	Primer sequence (F, R, 5′—3′)	oduct length (bp)
HPRT1	CCTGGCGTCGTGATTAGTG	125
	CAGTCCTGTCCATAATTAGTCC	
Runx2	GCCTTCAAGGTGGTAGCCC	67
	CGTTACCCGCCATGACAGTA	
Osteonectin	GGTATCTGTGGGAGCTAATC	224
	ATTGCTGCACACCTTCTC	
Osteocalcin	GCAAAGGTGCAGCCTTTGTG	80
	GCTCCCAGCCATTGATACAG	
PPARG	CGTGGCCGCAGAAATGAC	73
	CACGGAGCTGATCCCAAAGT	
UCP1	CGCAGGGAAAGAAACAGCAC	202
	GTCAAGCCTTCGGTTGTTG	

3.3.5 Statistical Analysis

Regression analysis was done using Graph-Pad Prism version 6.01 software (GraphPad Software, Inc.) to find the best-fit curve for layered porosities in structural characteristics simulation and a comparative study between simulated data obtained from image analysis and cell viability derived data from in vitro experience. Statistical analysis between structural characteristics and cell viability was implemented based on unpaired Student's t-test criteria. In addition, statistical analysis in biological tests was performed by SPSS software (IBM Corporation, USA), based on one-way ANOVA. Results are presented as means ± SD. Significance levels are *$p<0.05$, **$p<0.01$ and ***$p<0.001$. All the quantitative results were presented as mean and standard deviations.

4 RESULTS AND DISSCUTION

4.1. Solution properties of PAN/CNT

The results obtained from solution characterization revealed that viscosity is proportionally correlated to polymer concentration. Moreover, CNT is a low density and high surface area nanoparticle, and the solution viscosity rapidly increased with an incremental addition of CNT loads. Solution viscosity did not noticeably vary following the incorporation of plasticizer. Identical viscosities of samples containing EC can be attributed to the partial replacement of DMF (molar mass: 73.09 g/mol) with EC (molar mass: 88.06 g/mol) in the solution composition (Table 1).
The electrical resistance of 10 wt% polymer solutions decreased from 880 KΩ, to 500 KΩ by adding CNT up to 0.75 wt% (Figure 1). Such a small increase in conductivity suggests that PAN solutions with different CNT concentrations (up to 0.75 wt%) were below the electrical percolation threshold during the 30 min sonication time. The results from the measurement of electrical resistance confirmed that adding EC at 1–6 wt% did not induce significant changes in electrical conductivity (Figure 9).

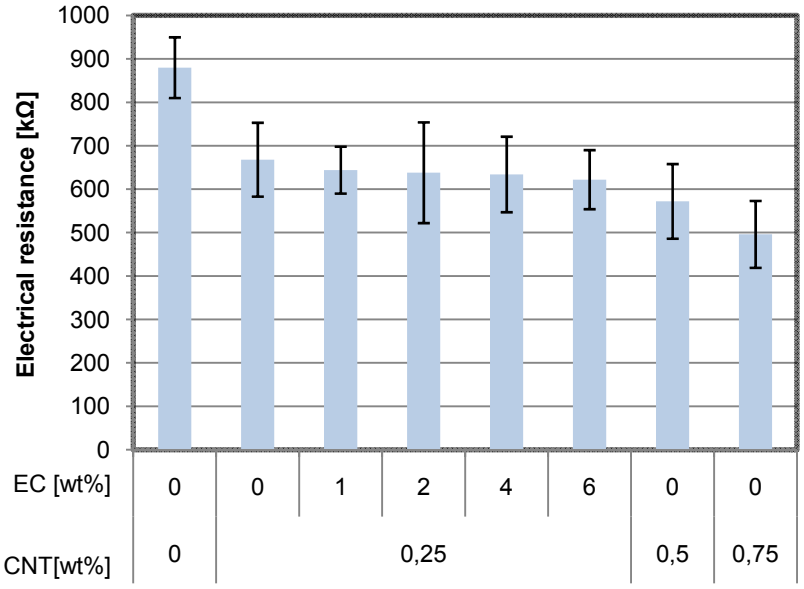

Figure 9. Mean electrical resistance of different CNT and EC loads in 10 wt% PAN

4.2. Effect of polymer concentration and carbon nanotube on morphology of PAN fibres

In electrospinning, polymer concentration and the corresponding viscosity should bring sufficient entanglement of the polymer chains. This requisite is of utmost importance for attaining smooth fibers, rather than solidified droplets, or beaded fibers. [50,156] Thus, as shown in Figure 10(a), the lowest concentration (6 wt %) had the highest tendency to form solidified droplets, whilst an increase of polymer concentration, gradually decreased the density of beads, and changed the shapes of beads from spheres to spindles (Figure 10(a)-10(b)).

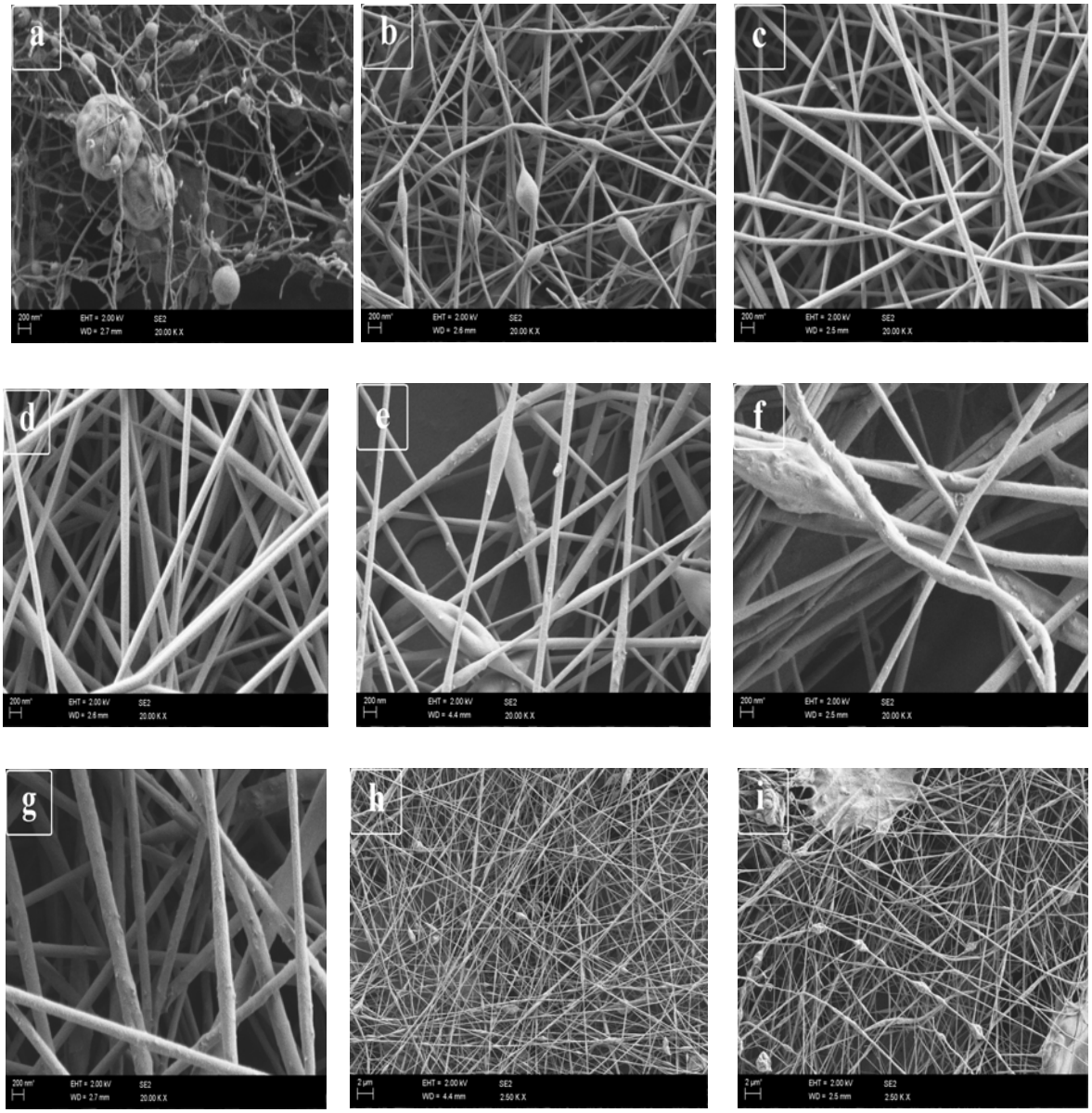

Figure 10. Appearance of pure PAN nanofibres with different polymer concentrations; a) PAN 6 wt%, b) PAN 8 wt%, c) PAN 10 wt%, d) PAN 12 wt% (magnification 20 kx). Appearance of PAN/CNT nanofibre composites; e) PAN 10

wt%, CNT 0.25 wt%, f) PAN 10 wt%, CNT 0.75 wt%, g) PAN 12 wt%, CNT 0.5 wt% (magnification 20 kx), h) PAN 10 wt%, CNT 0.25 wt%, i) PAN 10 wt%, CNT 0.75 wt% (magnification 2.5 kx).

In general, beads are formed due to aggregation of solvent molecules because of surface tension [54]. At high solution concentrations (chain entanglement), solvent molecules are distributed among entangled chains and their tendency to congregate in the form of beads is decreased [54]. The variation of shape and declining trend of bead structures at high polymer concentrations can also be attributed to dynamics of jet elongation. It could be suggested that increasing polymer concentration leads to a higher degree of chain entanglement and a longer relaxation time for the solution [156] and a longer relaxation time leads to higher solution elasticity. Increased elastic stress originating from solution elasticity causes a slowdown of Rayleigh instability and reduces the bead structures. Furthermore, complete suppression of Rayleigh instability leads to transition of the resultant morphology from bead structures to uniform fibers (Figure 10(c)-10(d)) [62].

Increasing the polymer concentration led to an increase in diameter of PAN fibers (Figure 11(a)). This trend may reflect the increasing resistance of viscous jet in stretching between the nozzles and target collector [54].

The addition of CNT in different concentrations into 10 wt% PAN solutions led to the formation of conical shaped beads along the fibres axes (Figure 10(e), 10(f), 10(h), and 10(i)). This phenomenon can be attributed to poor dispersion of CNT into the polymer solutions [157]. The fibers tended to become curly and the solution tended to drip on the electrospun web when the CNT loads were increased (Figure 10 (f), 2(i)).

Poor homogeneity, seen as an increase in the agglomeration of CNTs, induced structural irregularity to the electrospun web. When CNTs agglomerate, there is localised charge accumulation in the driven jet, resulting in an inhomogeneity of the electric field [158]. This phenomenon leads to the formation of beads and other structural irregularities due to different extensional stresses induced by the electrified jet. In addition to agglomeration of nanotubes based on the van der Waals attraction, CNT may also interact with nitrile groups of polymer [159]. This can cause a weakness of polymer chains interaction and results in a reduction of solution elasticity [160]. The reduced elasticity intensifies Rayleigh instability and leads to the formation of bead structures [62]. At high CNT loads, as a result of Rayleigh instability, solution drippings were deposited on the target collector in addition to beaded fibers (Figure 10(i)). Also, in a solution with 12 wt% PAN, 0.5 wt% CNT, smooth fibers were formed, whereas beaded fibers were produced at lower polymer concentrations (10 wt %), (Figure 10(g)). This phenomenon can be attributed to stabilization of the driven jet resulting in increasing entanglement of polymer chains at high polymer concentrations. This observation also confirmed the role of chain entanglements in the formation of beadless fibers even in presence of carbon nanotubes. Fiber diameter gradually increased as the CNT concentration increased. It appears that the viscosity of solution has a greater impact on fiber diameter than a slight increase in the electrical conductivity (Figure 11(b)).

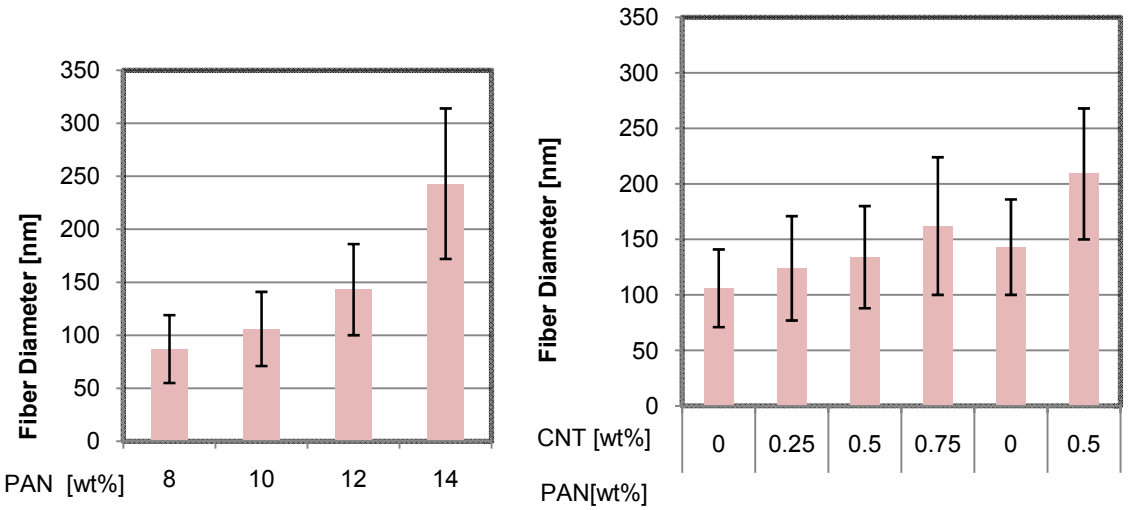

Figure 11. Mean fibre diameter of; a) PAN nanofibres with different polymer concentration, b) PAN nanofibres with different nanotube concentrations.

4.3 Effect of Ethylene Carbonate on Morphology of PAN/CNT Nanofibres

The addition of EC plasticiser into PAN/CNT solutions led to both the declining trend of fiber diameters and the formation of spherical shaped beads (Figure 12-13). As mentioned earlier, viscosity and solution conductivity remained almost constant, thus these morphological changes in the fibers containing EC must be due to reasons other than viscosity and conductivity. Inclusion of EC may form binary phases within the polymer solution, and agglomerate the CNT phase, thus affecting the elasticity and viscosity properties. The reduction of fibre diameters and formation of spherical shaped beads maybe a result of the stretching of low molecular weight EC-polymer phase over the nozzle-collector distance. Beyond phase separation, the nature of EC as a PAN plasticiser may cause these morphological variations. Based on gel theory of plasticisation, the polymer has a tridimensional honeycomb structure, formed by the loose attachment between polymer molecules along their chains [161]. A plasticiser works to reduce these weak intermolecular interactions, allowing the polymer to deform without breaking [161]. On the other hand, elasticity of polymer solutions is proportional to molecular weight and intermolecular interaction [162]. It is hypothesized that EC as a plasticiser reduces the interaction between the molecular chains, resulting in a reduction of solution elasticity and its elastic respond counterpart. The reduced elastic respond acts to intensify the Rayleigh instability and lead to an increase of bead structures and droplets in the electrospun web [62].

Variation in the shape of beads may also be related to competition between the elastic respond originating from solution elasticity, and Rayleigh instability driven by surface tension. Elastic respond tends towards a coherent jet [62] with spindle shapes and conversely, Rayleigh instability driven by surface tension, tends towards congregated droplets. Therefore, when the elasticity of the solution is decreased, large size spherical beads tend to appear instead of spindle-shapes. The slight reduction of fiber diameter in samples containing EC can be attributed to a lower resistance of the electrified jet against extensional deformation and capillary thinning mechanism, due to lower solution elasticity [62, 163].

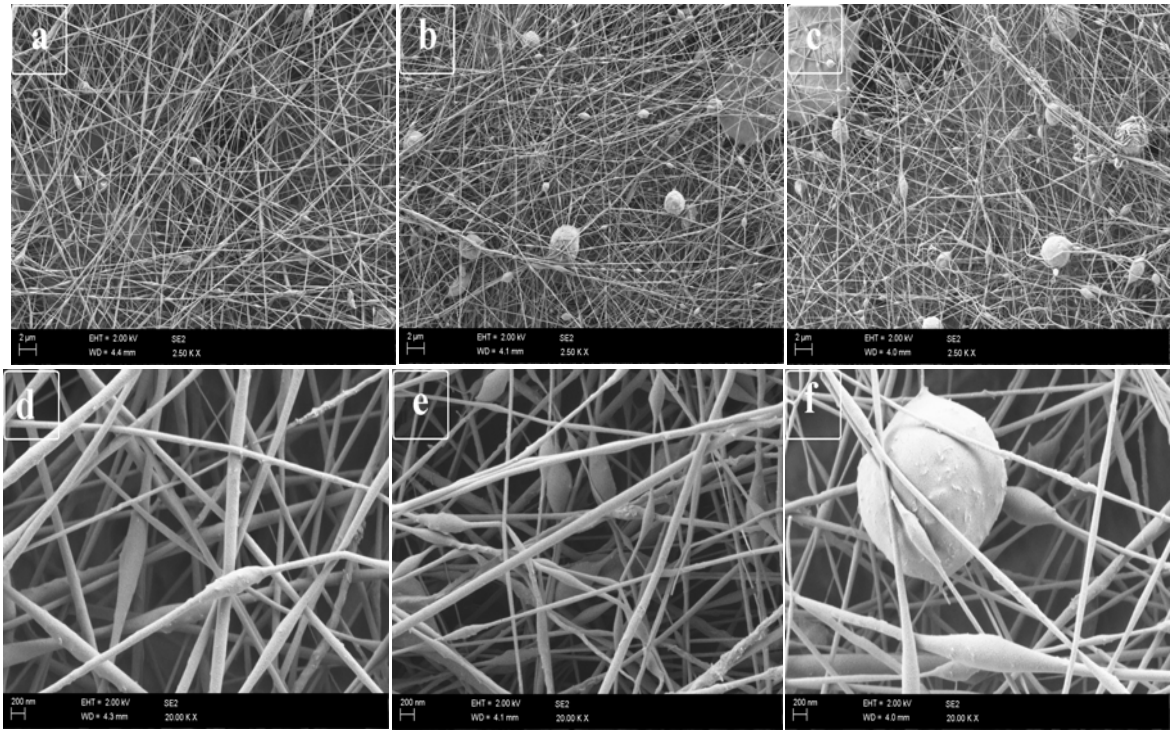

Figure 12. Appearance of PAN /CNT nanofiber composites with different plasticiser concentrations; a-d) 0 wt% EC, b-e) 4 wt% EC, c-f) 6 wt% EC (magnification 2.5 kx and 20 kx).

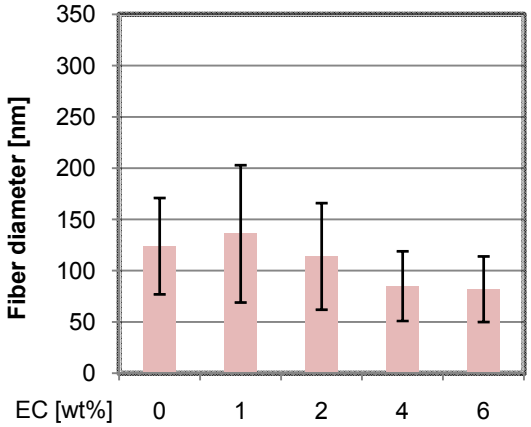

Figure 13. Mean fiber diameters of PAN nanofibers with different plasticiser concentrations in 10 wt% PAN and 0.25 wt% CNT load.

4.4 The Relation between Morphological Variations and Structural Characteristics (SPE, Porosity, Interconnectivity, Pore Size and Fiber Diameter)

As alluded to previously, pore interconnections are formed by random deposition of fibers during the electrospinning process. Based on this phenomenon, pore interconnectivity in electrospun membranes is correlated to the mechanism of fiber deposition and structural imperfections induced in the fibrous membrane. However, significance of each parameter on variation of interconnectivity is different and mostly depends on the induction degree of such imperfections. Structural imperfections can be classified in two main groups. Firstly, imperfections that partially influence the structural properties of the membrane; bead structure along the fiber axis and partial solution dripping can be included in this first category. Secondly, structural imperfections that interrupt the entire membrane structure and influence the overall characteristics of the membrane. Examples of the latter include high fiber size and low fiber deposition originating from fundamental processing parameters in electrospinning, leading to induction of a high degree of imperfections or structural differences in the membrane. To verify the proposed method, structural characteristics of seven samples with different morphological features were measured and ordered in accordance with their respective scaffold percolative efficiency (SPE), as shown in Figure 14. It was observed that the morphology and structure of the first four samples (1 to 4) came close to fulfilling the perfect criteria for depth filtration due to adequate fiber deposition. In contrast, the last three samples fell well short of these criteria due to low fiber deposition resulting largely from inappropriate processing parameters. The quantification of interconnectivity (see Figure 15(c)) revealed that interconnectivity was increased when fiber size was decreased. Membrane 1 compared to membrane 2 and membrane 3 compared to membrane 4 had a higher interconnectivity index, respectively, due to lower fiber size. On the contrary, in the case of overall porosity this trend was established inversely for the mentioned samples (Figure 15(b)). On this basis, fiber size was a

dominating factor in determining SPE (see Figures 15(a) and (e)), and may have outweighed the effect of lower overall porosity in the first four samples. This may be due to the influence of fiber size within entire membrane structures, whereas reduced porosity only partially influences the membrane structures due to beads and solution dripping (see Figures 14 (a)-(d)). As a consequence, the highest SPE belonged to sample 1 and this value decreased slightly from sample 2 to 4, respectively.

Although the differences between the measured values for mean SPE, interconnectivity and overall porosity seem to be insignificant in the first four samples, it should be noted that these values were obtained precisely through segmentation and simulation of arbitrary images at the nano scale. Furthermore, overall porosity was measured as the remaining open area after whole fibrous networks was projected in the 2D plane, and interconnectivity was evaluated based on limited numbers of cumulative layers. Thus, based on the proposed method, it seems that any slight difference in the value of structural elements results in considerable differences in depth filtration performance. In case of the latter three samples (see Figures 14(e)-(g)), it can be observed that sample 5 has higher pore interconnection and a greater accessible open area for depth filtration in comparison to samples 6 and 7. This trend was also reflected in their respective measurements. In addition, due to having the lowest fibre deposition, sample 7 (see Figure 14(g)) did not meet the structural requirement for depth filtration and, correspondingly, its SPE was considerably lower than the other membranes. Based on the discussion above, it was concluded that the results obtained on intrinsic structural properties are well compatible with empirical observations of perfect membrane structures.

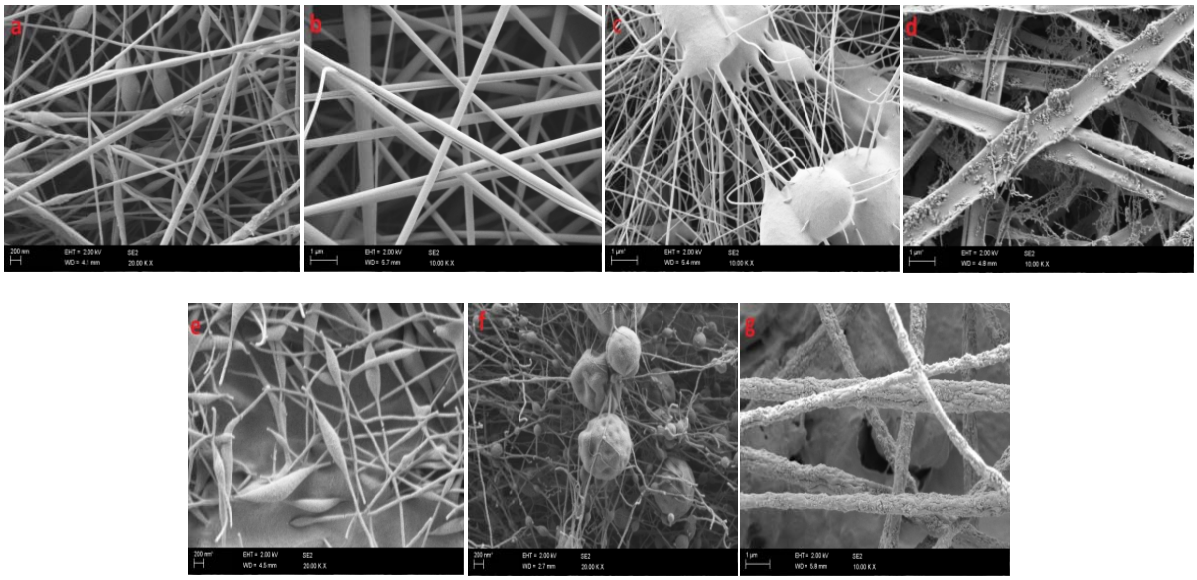

Figure 14. a-g) FESEM images captured from membrane samples 1- 7, respectively.

a, b, c)

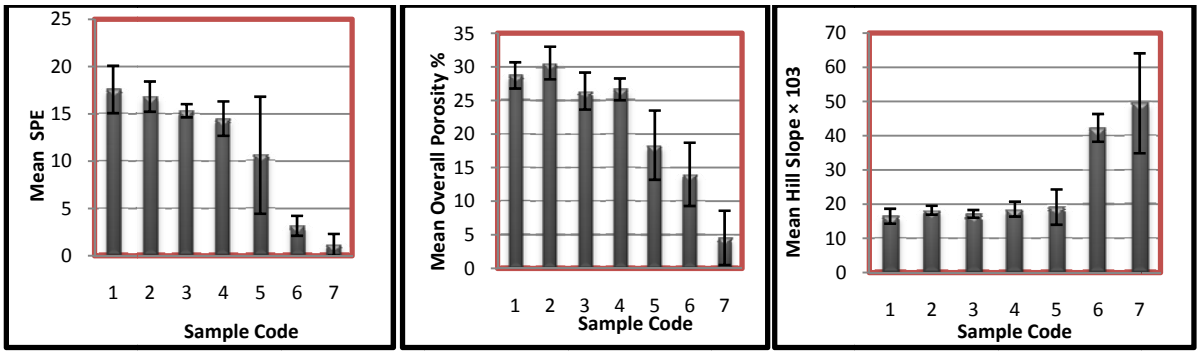

d, e)

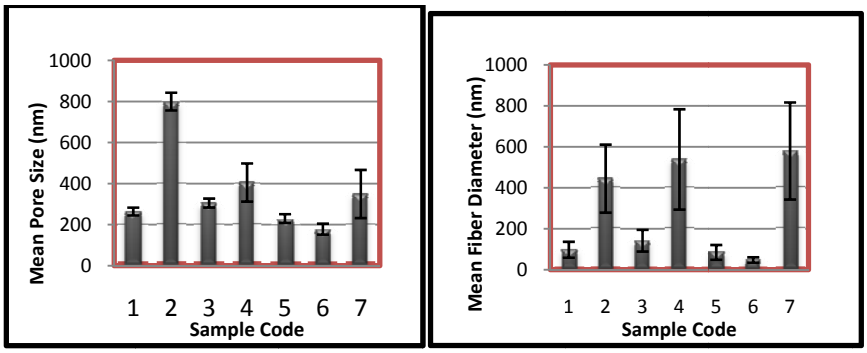

Figure 15. a) mean SPE, b) mean overall porosity, c) mean reciprocal interconnectivity (hill slope×10^3), d) mean pore size and e) mean fibre size of the sample membranes.

4.5 Evaluation of Depth Filtration (Infiltration) and Optimal Pore Size (OPS) in Nanofibrous Membrane

The $F(x)$ and OPS estimate the quality of depth filtration in terms of how the accessible channels of specific pore size are narrowed and block transport media in depth profile of the membrane. As previously described, the depth filtration elements are determined locally based on individual images captured from specific parts of the membrane. However, if the deposition of fibers is almost uniform, this evaluation can be extended to the entire membrane. The standard deviation of interconnectivity index and overall porosity can serve as rough indicators of the quality of fiber deposition, in that a higher standard deviation indicates higher non-uniformity of fiber deposition throughout the entire membrane. In contrast, a small standard deviation indicates that the deposition of fibrous network was almost uniform within the membrane. As Table 4 summarizes, the filtration elements such as $F(x)$ and OPS were measured locally based on the single sample images illustrated in Figures 6(a)-(g). Since the standard deviation of the interconnectivity index and overall porosity in the first four samples was small (see Figures 15(b) and (c)), the corresponding $F(x)$ and OPS can contribute to evaluation of the entire membrane.

Table 4. Best fitted curves F(x) for the layered porosities and their corresponding optimal pore size (OPS)

Image code	F(x)	OPS (nm)
a	$\frac{100}{1+10^{((4.98-x)\times 0.015)}}$	[274-467]
b	$\frac{100}{1+10^{((0.56-x)\times 0.018)}}$	[776-1024]
c	$\frac{100}{1+10^{((0.26-x)\times 0.016)}}$	[294-408]
d	$\frac{100}{1+10^{((-0.78-x)\times 0.020)}}$	[354-504]
e	$\frac{100}{1+10^{((2.54-x)\times 0.024)}}$	[226-428]
f	$\frac{100}{1+10^{((3.03-x)\times 0.040)}}$	[161-400]
g	$\frac{100}{1+10^{((0.38-x)\times 0.057)}}$	[272-410]

4.6 Relation between Structural Characteristics of Chitosan Nanofibrous Scaffold and Cell Viability

Although attaining defect-free fibrous scaffold from electrospinning of chitosan solution is a significant challenge, the appropriate viscoelasticity of driven jet led to the formation of smooth fibers without structural imperfections (beaded fibers and solution drippings). The morphologies of sample scaffolds after cross-linking with GA at different processing setups are shown in Figure 16. The observations of FE-SEM images revealed that there are no paramount morphological variations in different sample scaffolds that can be expressed qualitatively. On the other hand, the results obtained from MTT assay revealed that the chitosan/PEO scaffolds produced are not cytotoxic, because mean relative absorbance and thus mean cell viability are higher than half of the value attributed to the control sample (scaffold-free well). In addition, mean value of viable cells in different samples was enhanced from 50% to 110% compared to that belonging to the control (see Figure 17).The nanofibers constituting the 3D scaffold had a mean diameter between 170 and 320nm, while the mean pore sizes as well as overall porosity fraction varied between 330 and 790nm and between 0.11 and 0.32 in different samples, respectively. The differences between viable cells in the samples scaffold reflect the significant effects of structural characteristics in the mechanism of cell growth even at nanoscale. The results obtained from image analysis and simulations of structural characteristics are illustrated in Figure 17. Statistical hypothesis tests were implemented based on unpaired Student's t-test criteria for comparing two mean groups consisting of the mean values of relative absorbance versus mean fibers diameters, mean pores size, mean overall porosity, mean reciprocal interconnectivity index, and mean scaffold percolative efficiency separately. P values were obtained between relative absorbance and each structural element was smaller than 0.001 which shows that these parameters are highly statistically significant in cellular viability. Furthermore, to find the degree of correlation of each parameter with the number of viable cells, Pearson correlation coefficients were measured. The Pearson correlation coefficient for overall porosity and scaffold percolative efficiency were negative, which reveals that increasing porosity and scaffold percolative efficiency caused decreased number of viable cells, and vice versa. On the contrary,, Pearson correlation coefficient for pore and fiber size as well as reciprocal interconnectivity index were positive and showed an identical trend with regard to variations of viable cells. In the electrospinning process, fiber size has an inverse correlation with porosity, whereas pore size and fiber size show an identical trend [164-167]. In addition, based on our simulation [168], fiber size and reciprocal interconnectivity have a direct correlation. This means that fiber size and interconnectivity have an inverse correlation. This is due to the reduced size of fibers in the electrospun mat increasing the interconnectivity. From comparative analysis, it was found that the viability increased when percolative efficiency as a value obtained from dividing porosity on reciprocal interconnectivity was decreased (see equation (8)). Previous research has also shown that, by increasing fiber and thus pore size in the electrospun scaffold, the cellular infiltration and viability were enhanced [164, 169-170], and the comparative study also reflects these phenomena.

It is evident that packed surface morphologies and small pore sizes of the electrospun membrane hinder cellular permeation and attachment which leads to a reduction in viability.

This is because permeation of cells in 3D architecture of scaffolds was prevented. In this situation, an adhesion site along fibers is a more beneficial parameter for cell attachment and viability. On this basis, high fiber size and consequently larger pores for maintaining an adequate attachment site for interaction between cells and scaffold matrix are an appropriate condition for achieving maximum viability. Inversely, increased porosity based on small pore size reduces the interaction between cells and scaffold matrix.

To enhance the cell attachment in 3D scaffold, it is important that the cells diffuse in different layers in depth of the scaffold profile. If the scaffold has an optimal pore size, the interconnectivity of scaffold leads to permeated cells being able to take advantage of entire scaffold layers in depth profile. However, in the case of small pore sizes, the cell introduced can only interact with the surface layers of the scaffold. In this regard, if the layers are more packed in the depth of scaffold profile, the cells can take advantage of larger area of surface layers for attachments. Therefore, if interconnectivity decreases, the scaffold mostly exhibits 2D architecture, which is beneficial for surface cell attachment. It is because of the faster blocking of pores in the surface layers (low interconnectivity), which can provide a higher attachment site for cells and thus increase the viability. This phenomenon is also reflected in the statistical analysis in which reciprocal interconnectivity has an identical trend with viability, and the lower values of viability in some samples compared to control show these facts.

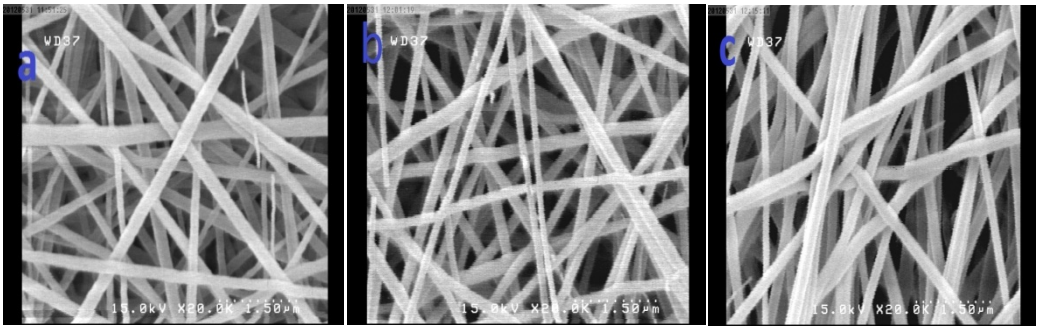

Figure 16. FE-SEM images in magnification of 20 kx, from nanofibrous scaffolds, a) sample 3 (variation on deposition time), b) sample 5 (variation on feed rate) and c) sample 7 (variation on voltage).

From the discussion above, the comparative analysis obtained from structural simulation and in vitro experiences are highly compatible with empirical and theoretical results attributed to structural elements and cellular viability in nanofibrous scaffolds. It can be concluded that the structural elements have significant impacts on cellular attachment and viability in the nanofibrous membrane. In addition, the size of porous structures and cells determined the quality of cellular permeation and interaction in the scaffold matrix. However, this quality can be enhanced by optimizing structural elements even at nanoscale, resulting from manipulation of processing parameters in electrospinning.

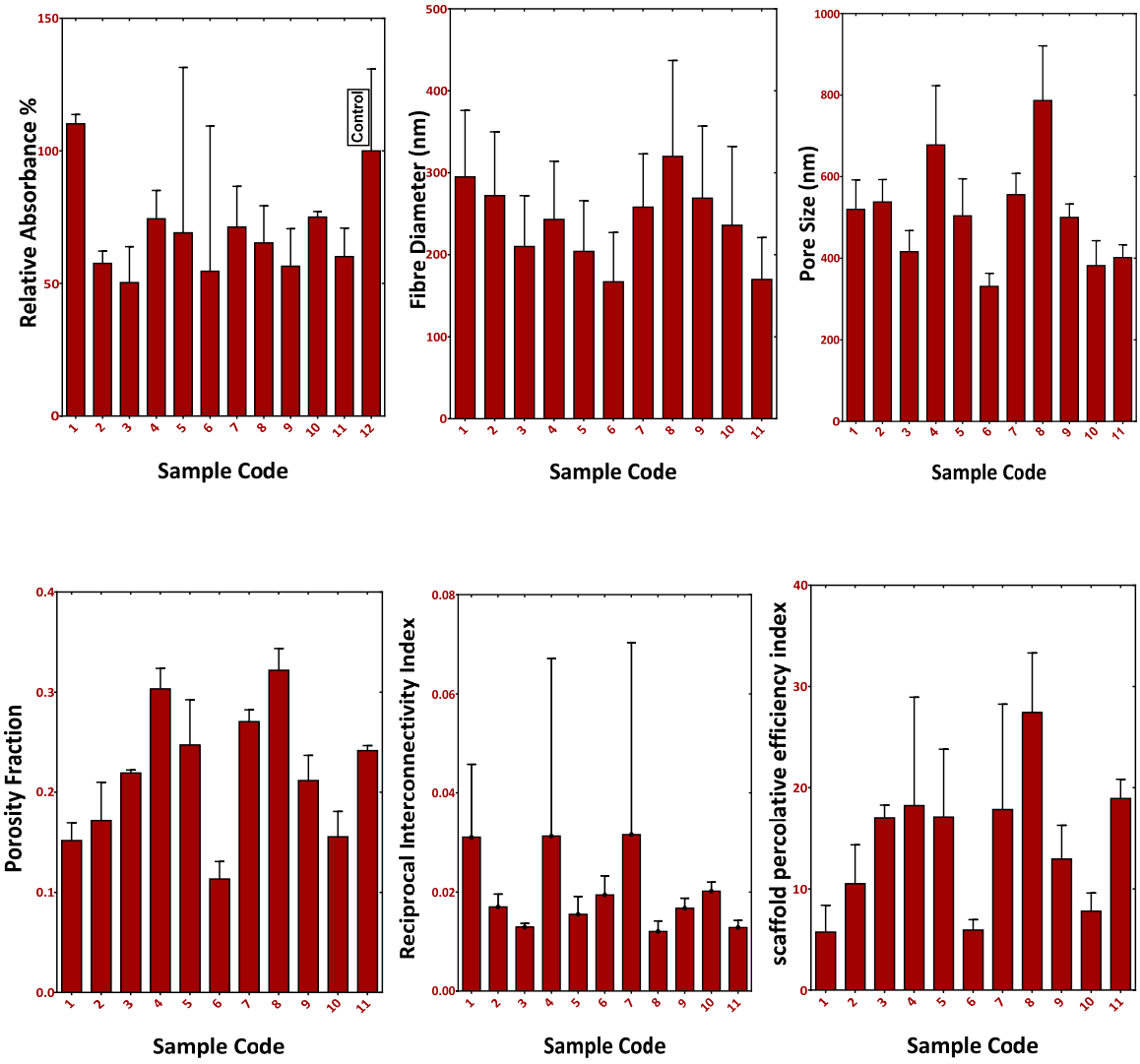

Figure 17. The diagrams of mean value of relative absorbance, fiber diameter, pore size, overall porosity fraction, reciprocal interconnectivity index and scaffold percolative efficiency for different sample scaffolds respectively. P values smaller than 0.001 were considered statistically significant in unpaired student's t-test.

4.7 Effect of Nanofiber Coating on Viability and Proliferation Rate of Mesenchymal Stem Cells

High deposition time in electrospinning leads to a gradual decrease in the inner diameters of pore channels and thus disrupts the infiltration of cells and mass transformation into hybrid scaffold. On this basis, in the present work, a short deposition time (300 sec) was chosen in order to favor the formation of low density chitosan/PEO fibrous coating on the surface of commercial scaffold. Other processing parameters were selected in optimal conditions in order to form continuous fibers without any structural imperfections. SEM images including commercial scaffold, commercial scaffold with seeded MSCs and hybrid scaffold (MNHS) with seeded MSCs were taken (Figure 18). These images revealed that in the absence of fibrous coating, MSCs only attached to the surface of PS scaffold, but they were able to

attach both to the surface and connection bridges when hybrid scaffold was used (Figure 18(c)). Cell viability and proliferation rate of MSCs were evaluated by colorimetric assay using MTT as a chemical to enter into mitochondria of viable cells and produce formazan crystals in presence of succinate dehydrogenase. This phenomenon was also confirmed by DAPI images, where showed more viable cells were recognized in hybrid scaffold (Figure 19). As shown in Figure 20, proliferation rate of MSCs was increased in hybrid scaffold during a period of 6 days in a time dependent manner. This may be due to the higher resemblance of the structure and components of hybrid scaffold to native ECM. On the other hand, it appears that the inclusion of chitosan/PEO nanofiber may also induce higher hydrophilic characteristics, as well as providing cell-recognition domains, leading to increased cell-scaffold interaction in MNHS. Furthermore, increased attachment, viability and proliferation in MNHS may indicate exploitation of the higher surface area to volume ratio, resulting in nano features of the scaffold, whereas the nanofibers formed the connection bridges between PS microfibers. In addition, MSCs in presence of nano-fibrous networks may tend to have a more stretched morphology, as well as a higher spreading and lower degree of cell aggregation, resulting in enhanced proliferation of cells [171-172].

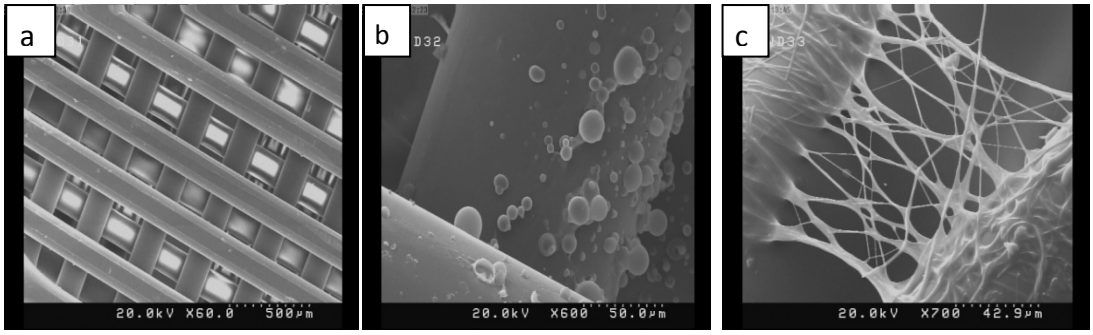

Figure 18. SEM images of morphology of scaffolds used in this study:a) 3D commercial microfiber scaffold without MSCs (magnification 60x); b) 3D commercial microfiber PS scaffold seeded with MSCs (magnification 600x); c) 3D Hybrid scaffold (commercial PS microfiber scaffold+ low deposition of Cs/PEO nanofiber) seeded MSCs (magnification 700x)

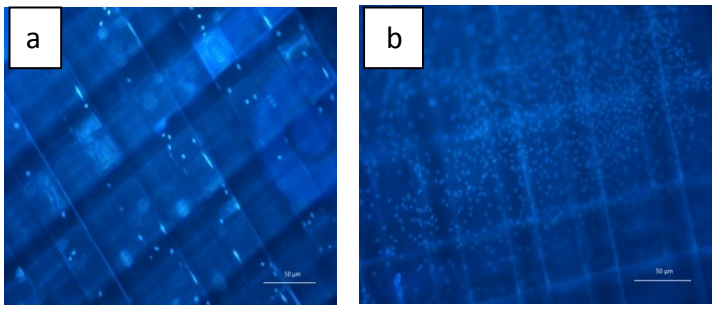

Figure 19. DAPI -stained fluorescence microscopic images of MSCs seeded on scaffolds (magnification 100x): a) 3D commercial seeded MSCs scaffold; b) 3D hybrid scaffold (MNHS) seeded MSCs. A higher attachment density was observed with MNHS

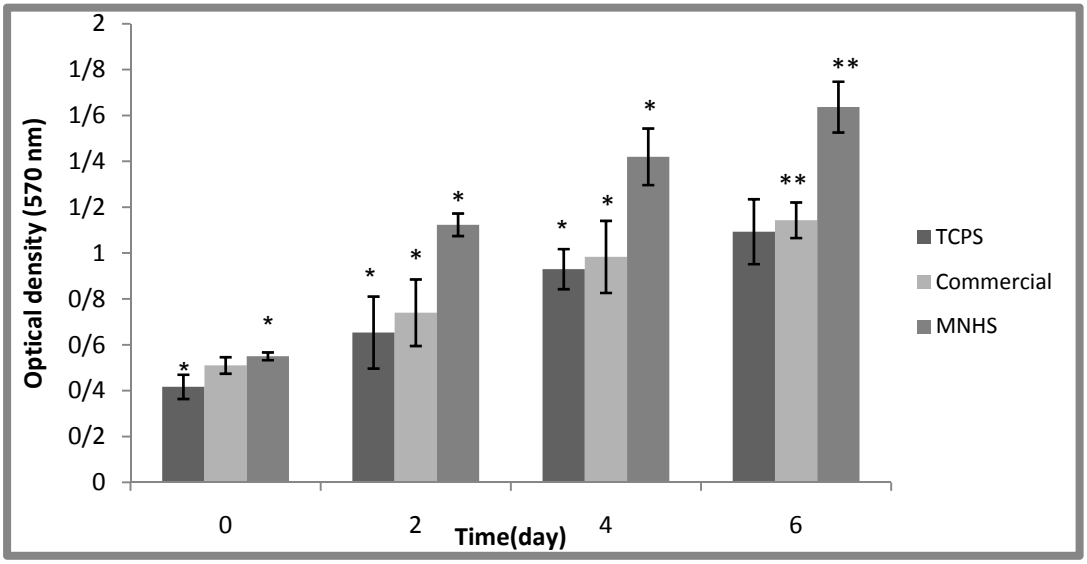

Figure 20. The proliferation rate of MSCs on TCPS, commercial PS scaffold and hybrid scaffolds (MNHS) during 0, 2, 4, and 6 days. Results are presented as means ± SD (n=3). Intra-day differences between TCPS, commercial and hybrid scaffolds were significant for days 2, 4 and 6 ($^{*}P<0.05$ and $^{**}P<0.01$, respectively).

4.8 Effect of Nanofiber Coating on Differentiations of Mesenchymal Stem Cells

The possibility of MSCs differentiation into both osteoblasts and adipocytes lineages was visually confirmed by images obtained from Alizarin Red and Oil Red-O staining as shown in Figure 21. Alizarin red was used as a marker for formation of calcified extracellular matrix in osteogenic differentiation, whereas Oil Red-O was utilized for staining adipocytes intracellular lipid vesicles in adipogenic differentiation.

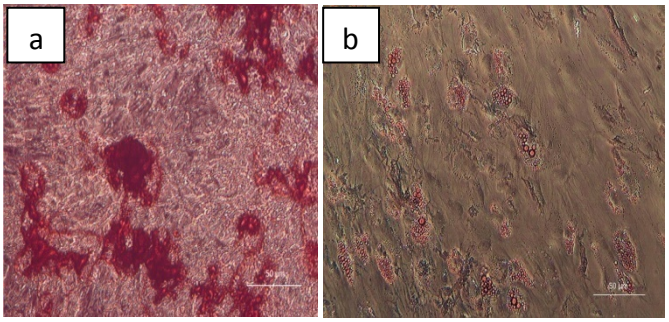

Figure 21. Staining Images after osteogenic and adipogenic differentiation. Alizarin Red staining for mineral deposition (left) and Oil Red -O staining for adipocytes intracellular lipid vesicles after adipogenic differentiation (right), were performed for MSCs. Images were recorded by a Nikon TE2000 fluorescent microscope (USA) at magnification of 100X.

4.8.1 Effect of Nanofiber Coating on Osteogenic Differentiations of Mesenchymal Stem Cells

Alkaline phosphatase is an ectoenzyme produced by osteoblasts and can be used as a marker for osteoblast activity. It maintains the concentration of phosphate or inorganic pyrophosphate for initiating the mineralization process [110].The data showed that the hybrid scaffold expressed a higher level of ALP activity than those of commercial and TCPS. The order of this activity was MNHS> commercial> TCPS (Figure 22(a)). Since ALP activity can

also be a marker for other lineages besides osteogenic differentiation, we used calcium content assay for osteogenic differentiation [112, 173-174]. Increased calcium deposition in MNHS indicated that the osteogenic differentiation was enhanced by coating of nanofiber on commercial scaffold.

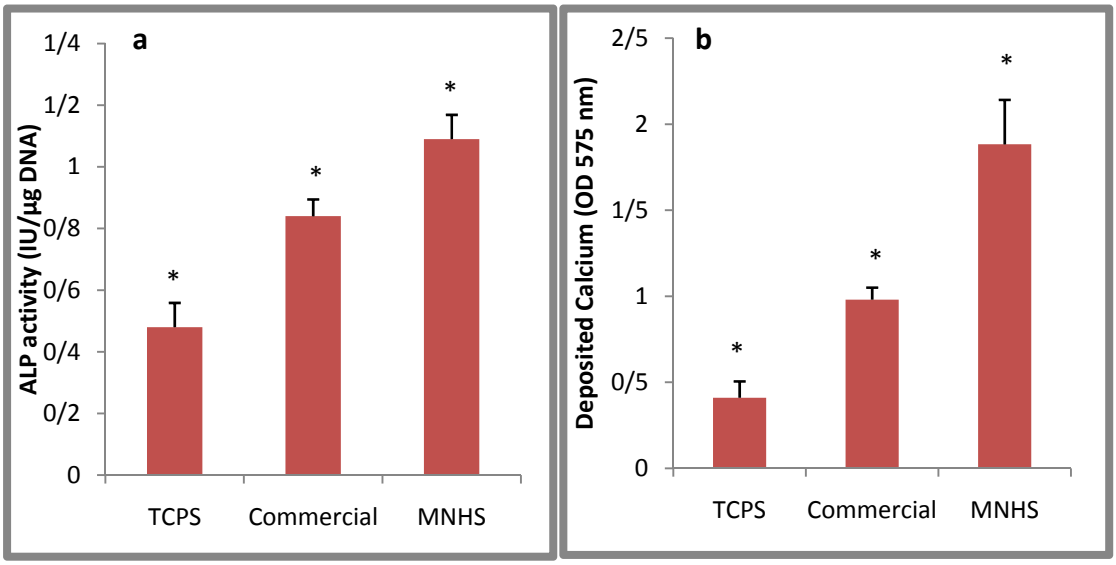

Figure 22. a) ALP activity and b) calcium content of MSCs seeded to TCPS, commercial PS scaffold and hybrid scaffold (MNHS). Results are presented as means ± SD (n=3.) Differences between the three samples were significant ($^{*}P<0.05$) for ALP activity and calcium content of MSCs grown on each sample.

Three important bone-related genes, including Runt-related transcription factor 2 (Runx2), osteonectin and osteocalcin were demonstrated by quantitative RT-PCR analysis to indicate better evaluation of the osteogenic differentiation of MSCs seeding in MNHS. As a transcription factor, Runx2 plays a significant role in the orientation of osteoprogenitors and stem cells towards osteolineage [175-176]. In addition, this factor prominently enables the regulation of osteoblast differentiation and maturation [177-179]. As a glycoprotein, osteonectin establishes bonds with Ca^{2+}, hydroxyapatite and type I collagen and manipulates the initial stages of crystal growth and cell-matrix interactions [176, 180]. Osteocalcin a bone Gla protein also known as bone gamma-carboxyglutamic acid-containing protein (BGLAP), which is associated with calcium binding [110]. As shown in Figure 23, higher levels of Runx2, osteonectin and osteocalcin were expressed in MNHS compared to commercial PS scaffold and TCPS after both 7 and 14 days. Also, the expression of these genes in PS scaffold was higher than that of TCPS. This can be attributed to the facts that chitosan nanofibers facilitate human osteoblast mineralization and maturation leads to higher expression levels of ALP, Runx2, osteonectin and osteocalcin genes expression in bone tissue regeneration [177, 181].

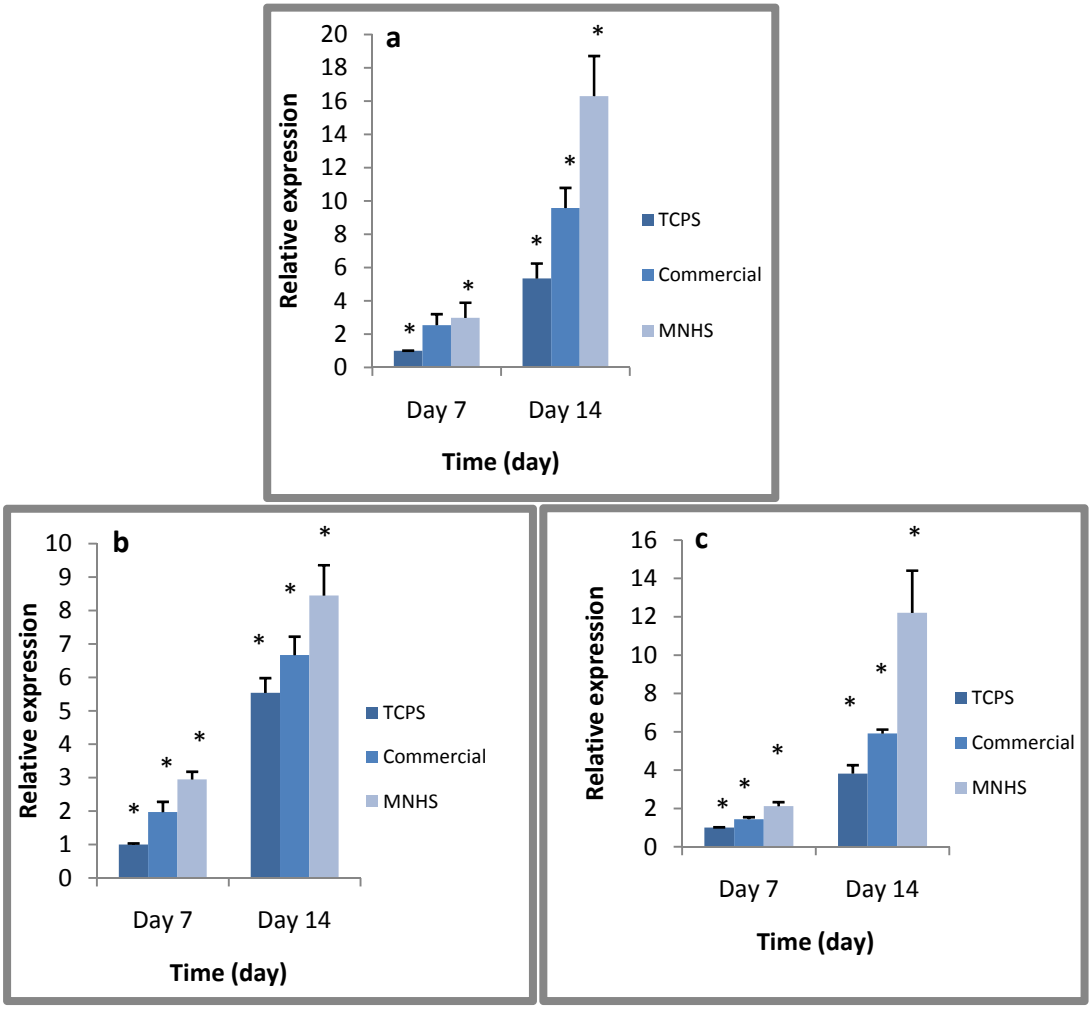

Figure 23. Real-Time RT-PCR analysis results. The relative quantification of a) Runx2, b) osteonectin, c) osteocalcin gene expression in differentiated MSCs seeded on commercial PS scaffold, MNHS scaffold and TCPS performed at 7 and 14 days. Results are presented as means ± SD (n=3). Intra-day differences between all tested samples were significant at 7 or 14 days ($^{*}P<0.05$).

4.8.2 Effect of Nanofiber Coating on Adipogenic Differentiations of Mesenchymal Stem Cells

As mentioned earlier, only a few publications have addressed the commitment of MSCs seeded in nano-fibrous scaffolds for adipogenic differentiation [109,114]. Here, it is important to assess whether the combination of commercial microfiber PS coated by chitosan/PEO nanofibers can meet analogy requirements for adipogenic differentiation. For this purpose, the quantitative analyses of Oil red- O staining in differentiated cells for 14 days and Real time PCR for adipo-gene expression for 7 and 14 days were performed. Adipo-gene expression consists of peroxisome proliferator activator receptor gamma (PPARγ), which is associated with white and brown adipose tissue [182], and uncoupling protein UCP1, a brown fat-specific marker [183]. PPARγ enhances HIB-1B brown adipocyte differentiation and up-regulates UCP-1gene expression [182, 184-185]. It was observed that both Oil Red- O staining and adipo- gene expressions of PPARγ and UCP1were significantly promoted in MNHS compared with commercial scaffold and TCPs, respectively (see Figure 24). These results confirmed that the coating of chitosan/PEO nanofibers on BioTek commercial scaffold enhanced adipogenic differentiation. Similar to osteogenic differentiation, increasing adipogenic differentiation may be attributed to chemicals and structural resemblances in MNHS scaffold compared to native ECM.

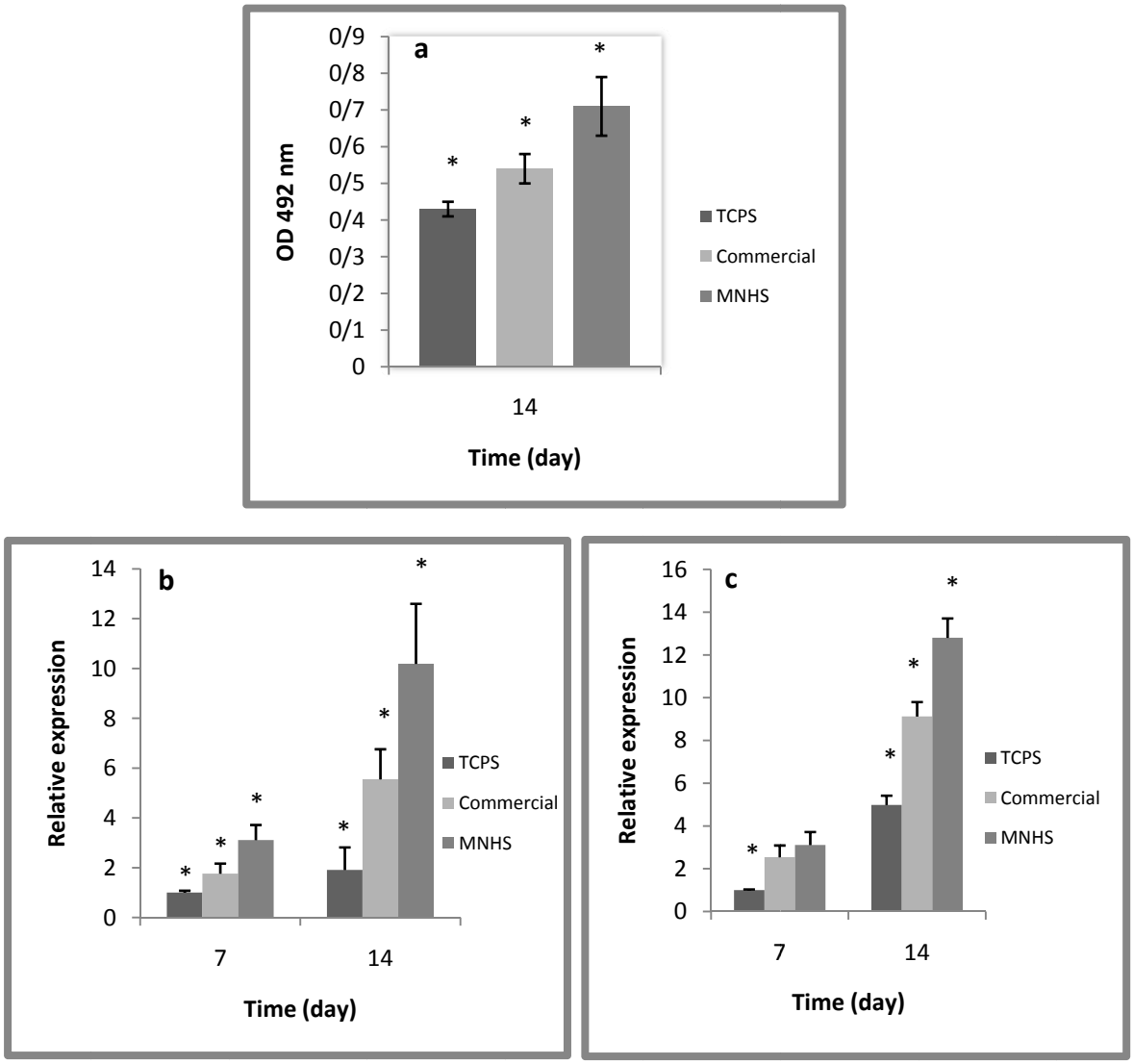

Figure 24. a)Qualitative Oil Red-O staining at 14 days; Real-Time RT-PCR analysis results, the relative quantification of b) PPARγ. c) UCP1 gene expression in differentiated MSCs seeded on commercial PS scaffold, MNHS scaffold and TCPS were performed at 7 and 14 days. Results are presented as means ± SD (n=3). Intra-day differences between all tested samples were significant at 7 or 14 days ($^{*}P<0.05$).

5 Conclusions

Extracellular matrix (ECM) plays an important role in tissue regeneration due to its modulating impacts on the adherence, viability, proliferation, differentiation and self-renewal of stem cells. In addition to biophysical and biochemical analogies, introducing a scaffold with the highest structural similarity to ECM can provide better compliance with stem cell behavior. Many investigations have been conducted for the preparation and characterization of three dimensional scaffolds fulfilling the required architecture of ECM in micro-environments.

Electrospinning is a simple and cost-effective fabrication method for producing a 3D fibrous network, from a wide variety of polymers, in submicron diameters. Accordingly, it has been utilized for producing the scaffolds for tissue engineering. Although electrospun fibrous scaffolds have many structural resemblances to ECM, their structural features have many impacts in their applications.

In this thesis, it was observed that an increase in polymer concentration leads to an increase in fiber diameters and reduction of bead density in electrospun nanofibers. The fiber diameters increased proportionally with filler (carbon nanotube) concentrations up to percolation threshold. The nanocomposite fibers exhibited different structures based on filler and polymer concentrations. The addition of plasticizer into polymer/filler solutions led to slight reduction in fiber diameters and the formation of spherical shaped beads. The inclusion of plasticizer induced similar morphological variations to the electrospun fibers regardless of its conductivity and viscosity impacts.

Furthermore, the structural characteristics such as pore size, porosity, pore interconnectivity and scaffold percolative efficiency of electrospun scaffold were simulated by image analysis. The proposed method can be applied to different morphological conditions even at high degrees of structural imperfection (low fiber deposition, beading and solution dripping). The reliability of the proposed approach was validated with measurements and comparison of the structural characteristics of several samples with different morphological architectures. The results and subsequent comparison were well compatible with empirical observations of perfect membrane structures.

Mouse fibroblast cells were cultured on different samples of 3D nanofibrous chitosan/ PEO scaffolds produced by manipulation of processing parameters in electrospinning. The cell viability was assessed by MTT assay. The results obtained from the MTT assay showed that nanofibrous chitosan/PEO scaffolds were not cytotoxic. A comparative study between the structural properties and viability of cells revealed that the packed morphology of sample scaffolds hinders cellular infiltration and attachment. However, the mean cellular viability rose from 50 to 110% compared to that belonging to the control even at narrow distributions of mean fiber diameter and pore size from 170 to 320 nm and 330 to 790 nm, respectively. In addition, it was observed that cell attachment and viability were enhanced by increasing fiber size and pore size, whereas on the contrary, this trend was the opposite for overall porosity, interconnectivity and scaffold percolative efficiency. This may be due to increased fiber diameter and thus pore size increasing the permeation and attachment of cells, while the other

parameters to some extent act inversely in electrospun scaffolds. Furthermore, the results obtained from the comparative study were highly compatible with empirical and theoretical concepts attributed to electrospun nanofibrous scaffold and cell viability in tissue engineering.

In addition, micro-nanostructured hybrid scaffold (MNHS) was tested as a three dimensional novel scaffold constructed by mild coating of chitosan/PEO nanofibers on commercial BioTek PS scaffold. It was observed that inclusion of nanofiber coating on the surface of commercial scaffold promoted the attachment, viability and proliferation rate of MSC seeded on MNHS. In addition, MNHS can be utilized as a scaffold for osteogenic and adipogenic differentiation. Results obtained from RT-PCR confirmed that chitosan/PEO nanofiber coating led to promotion of the expression level of Runx2, osteonectin and osteocalcin in osteogenic differentiation, as well as increasing the level of PPARγ and UCP1 expression in adipogenic differentiations. This enhancement could contribute to higher biochemical analogies and structural resemblance in hybrid scaffold. From this study, it can be concluded that combination of micro-porosity and nano-fibrous structure in the form of hybrid scaffold can promote MSCs behavior. Moreover, biocompatible MNHS can be used as a convenient scaffold for proliferation and differentiation of MSCs into bone and connective tissues.

References

1. Yang, S., Leong, K.F., Du, Z. and Chua, C.K., 2001. The design of scaffolds for use in tissue engineering. Part I. Traditional factors. *Tissue engineering*, *7*(6), pp.679-689.
2. U.S. Scientific Registry for Organ Transplantation and the Organ Procurement and Transplant Network. AnnualReport. Richmond VA: UNOS, 1990
3. Vacanti, J., and Vacanti, C. The challenge of tissue engineering. In: Lanza, R.P., Langer, R., and Chick, W.L., eds. Principles of Tissue Engineering. Austin, TX: Academic Press, 1997, pp. 1–6.
4. Karp, Jeffrey M., and Robert Langer. "Development and therapeutic applications of advanced biomaterials." *Current opinion in biotechnology* 18, no. 5 (2007): 454-459.
5. Langer, Robert, and David A. Tirrell. "Designing materials for biology and medicine." *Nature* 428, no. 6982 (2004): 487-492.
6. Chan, B. P., and K. W. Leong. "Scaffolding in tissue engineering: general approaches and tissue-specific considerations." *European spine journal* 17, no. 4 (2008): 467-479.
7. Bettinger, Christopher J., Robert Langer, and Jeffrey T. Borenstein. "Engineering substrate topography at the micro-and nanoscale to control cell function." *Angewandte Chemie International Edition* 48, no. 30 (2009): 5406-5415.
8. Wolf, Katarina, Regina Müller, Stefan Borgmann, Eva-B. Bröcker, and Peter Friedl. "Amoeboid shape change and contact guidance: T-lymphocyte crawling through fibrillar collagen is independent of matrix remodeling by MMPs and other proteases." *Blood* 102, no. 9 (2003): 3262-3269.

9. Friedl, Peter. "Prespecification and plasticity: shifting mechanisms of cell migration." *Current opinion in cell biology* 16, no. 1 (2004): 14-23.
10. Dent, Erik W., and Frank B. Gertler. "Cytoskeletal dynamics and transport in growth cone motility and axon guidance." *Neuron* 40, no. 2 (2003): 209-227
11. Yang, Shoufeng, Kah-Fai Leong, Zhaohui Du, and Chee-Kai Chua. "The design of scaffolds for use in tissue engineering. Part I. Traditional factors." *Tissue engineering* 7, no. 6 (2001): 679-689.
12. Shi, Jinjun, Alexander R. Votruba, Omid C. Farokhzad, and Robert Langer. "Nanotechnology in drug delivery and tissue engineering: from discovery to applications." *Nano letters* 10, no. 9 (2010): 3223-3230.
13. Huang, Jinghuan, Stefan V. Grater, Francesca Corbellini, Sabine Rinck, Eva Bock, Ralf Kemkemer, Horst Kessler, Jiandong Ding, and Joachim P. Spatz. "Impact of order and disorder in RGD nanopatterns on cell adhesion." *Nano Letters* 9, no. 3 (2009): 1111-1116.**2009**, *9*, 1111–1116.
14. Park, Jung, Sebastian Bauer, Klaus von der Mark, and Patrik Schmuki. "Nanosize and vitality: TiO2 nanotube diameter directs cell fate." *Nano letters* 7, no. 6 (2007): 1686-1691.
15. Xu, C. Y., R. Inai, M. Kotaki, and S. Ramakrishna. "Aligned biodegradable nanofibrous structure: a potential scaffold for blood vessel engineering."*Biomaterials* 25, no. 5 (2004): 877-886.
16. Norman, James J., and Tejal A. Desai. "Methods for fabrication of nanoscale topography for tissue engineering scaffolds." *Annals of biomedical engineering* 34, no. 1 (2006): 89-101.
17. Yim, Evelyn KF, Stella W. Pang, and Kam W. Leong. "Synthetic nanostructures inducing differentiation of human mesenchymal stem cells into neuronal lineage." *Experimental cell research* 313, no. 9 (2007): 1820-1829.
18. Dalby, Matthew J., Mathis O. Riehle, Stephen J. Yarwood, Chris DW Wilkinson, and Adam SG Curtis. "Nucleus alignment and cell signaling in fibroblasts: response to a micro-grooved topography." *Experimental cell research* 284, no. 2 (2003): 272-280.
19. Choi, Chang-Hwan, Sepideh H. Hagvall, Benjamin M. Wu, James CY Dunn, and Ramin E. Beygui. "Cell interaction with three-dimensional sharp-tip nanotopography." *Biomaterials* 28, no. 9 (2007): 1672-1679.
20. Yim, Evelyn KF, Stella W. Pang, and Kam W. Leong. "Synthetic nanostructures inducing differentiation of human mesenchymal stem cells into neuronal lineage." *Experimental cell research* 313, no. 9 (2007): 1820-1829.
21. Gerecht, Sharon, Christopher J. Bettinger, Zhitong Zhang, Jeffrey T. Borenstein, Gordana Vunjak-Novakovic, and Robert Langer. "The effect of actin disrupting agents on contact guidance of human embryonic stem cells." *Biomaterials* 28, no. 28 (2007): 4068-4077.
22. Dalton, B., X. Frank Walboomers, Mark Dziegielewski, Margaret DM Evans, Sarah Taylor, John A. Jansen, and John G. Steele. "Modulation of epithelial tissue and cell migration by microgrooves." *Journal of biomedical materials research* 56, no. 2 (2001): 195-207.
23. Bettinger, Christopher J., Zhitong Zhang, Sharon Gerecht, Jeffrey T. Borenstein, and Robert Langer. "Enhancement of in vitro capillary tube formation by substrate nanotopography." *Advanced Materials* 20, no. 1 (2008): 99-103

24. Li, Dan, and Younan Xia. "Electrospinning of nanofibers: reinventing the wheel?." *Advanced materials* 16, no. 14 (2004): 1151-1170.
25. Li, Wan-Ju, Cato T. Laurencin, Edward J. Caterson, Rocky S. Tuan, and Frank K. Ko. "Electrospun nanofibrous structure: a novel scaffold for tissue engineering." *Journal of biomedical materials research* 60, no. 4 (2002): 613-621.
26. Ma, Zuwei, Masaya Kotaki, Ryuji Inai, and Seeram Ramakrishna. "Potential of nanofiber matrix as tissue-engineering scaffolds." *Tissue engineering* 11, no. 1-2 (2005): 101-109.
27. Heikkilä, Pirjo. *Nanostructured Fibre Composites, and Materials for Air Filtration*. 2008.
28. Romeo, Valentina, Giuliana Gorrasi, Vittoria Vittoria, and Ioannis S. Chronakis. "Encapsulation and exfoliation of inorganic lamellar fillers into polycaprolactone by electrospinning." *Biomacromolecules* 8, no. 10 (2007): 3147-3152.
29. Heikkilä, P., and A. Harlin. "Electrospinning of polyacrylonitrile (PAN) solution: Effect of conductive additive and filler on the process." *Express Polymer Letters* 3, no. 7 (2009): 437-445.
30. Elsdale, Tom, and Jonathan Bard. "Collagen substrata for studies on cell behavior." *The Journal of cell biology* 54, no. 3 (1972): 626-637.
31. Bhattarai, Narayan, Zhensheng Li, Dennis Edmondson, and Miqin Zhang. "Alginate-based nanofibrous scaffolds: Structural, mechanical, and biological properties." *Advanced Materials* 18, no. 11 (2006): 1463-1467.
32. Barnes, Catherine P., Scott A. Sell, Eugene D. Boland, David G. Simpson, and Gary L. Bowlin. "Nanofiber technology: designing the next generation of tissue engineering scaffolds." *Advanced drug delivery reviews* 59, no. 14 (2007): 1413-1433.
33. Min, Byung-Moo, Young You, Jin-Man Kim, Seung Jin Lee, and Won Ho Park. "Formation of nanostructured poly (lactic-co-glycolic acid)/chitin matrix and its cellular response to normal human keratinocytes and fibroblasts."*Carbohydrate Polymers* 57, no. 3 (2004): 285-292.
34. Nishida, T., K. Yasumoto, T. Otori, and J. Desaki. "The network structure of corneal fibroblasts in the rat as revealed by scanning electron microscopy."*Investigative ophthalmology & visual science* 29, no. 12 (1988): 1887-1890.
35. Jia, Jun, Yuan-Yuan Duan, Jian Yu, and Jian-Wei Lu. "Preparation and immobilization of soluble eggshell membrane protein on the electrospun nanofibers to enhance cell adhesion and growth." *Journal of Biomedical Materials Research Part A* 86, no. 2 (2008): 364-373.
36. Ma, Zuwei, Masaya Kotaki, Ryuji Inai, and Seeram Ramakrishna. "Potential of nanofiber matrix as tissue-engineering scaffolds." *Tissue engineering* 11, no. 1-2 (2005): 101-109.
37. Yoshimoto, H., Y. M. Shin, H. Terai, and J. P. Vacanti. "A biodegradable nanofiber scaffold by electrospinning and its potential for bone tissue engineering." *Biomaterials* 24, no. 12 (2003): 2077-2082.
38. Zhang, Yanzhong, Hongwei Ouyang, Chwee Teck Lim, Seeram Ramakrishna, and Zheng-Ming Huang. "Electrospinning of gelatin fibers and gelatin/PCL composite fibrous scaffolds." *Journal of Biomedical Materials Research Part B: Applied Biomaterials* 72, no. 1 (2005): 156-165.

39. Huang, Lei, Karthik Nagapudi, Robert P. Apkarian, and Elliot L. Chaikof. "Engineered collagen–PEO nanofibers and fabrics." *Journal of biomaterials science, Polymer edition* 12, no. 9 (2001): 979-993.
40. Kumbar, S. G., R. James, S. P. Nukavarapu, and C. T. Laurencin. "Electrospun nanofiber scaffolds: engineering soft tissues." *Biomedical Materials* 3, no. 3 (2008): 034002
41. Kim, Geun Hyung. "Electrospun PCL nanofibers with anisotropic mechanical properties as a biomedical scaffold." *Biomedical materials* 3, no. 2 (2008): 025010.
42. Dilamian, M., Montazer, M., & Masoumi, J. (2013). Antimicrobial electrospun membranes of chitosan/poly (ethylene oxide) incorporating poly (hexamethylene biguanide) hydrochloride. *Carbohydrate polymers*, *94*(1), 364-371.
43. Charernsriwilaiwat, Natthan, Praneet Opanasopit, Theerasak Rojanarata, and Tanasait Ngawhirunpat. "Lysozyme-loaded, electrospun chitosan-based nanofiber mats for wound healing." *International Journal of Pharmaceutics*427, no. 2 (2012): 379-384.
44. Taepaiboon, Pattama, Uracha Rungsardthong, and Pitt Supaphol. "Vitamin-loaded electrospun cellulose acetate nanofiber mats as transdermal and dermal therapeutic agents of vitamin A acid and vitamin E." *European Journal of Pharmaceutics and Biopharmaceutics* 67, no. 2 (2007): 387-397.
45. Taepaiboon, Pattama, Uracha Rungsardthong, and Pitt Supaphol. "Drug-loaded electrospun mats of poly (vinyl alcohol) fibres and their release characteristics of four model drugs." *Nanotechnology* 17, no. 9 (2006): 2317.
46. Megelski, Silke, Jean S. Stephens, D. Bruce Chase, and John F. Rabolt. "Micro-and nanostructured surface morphology on electrospun polymer fibers." *Macromolecules* 35, no. 22 (2002): 8456-8466.
47. Lee, K. H., H. Y. Kim, H. J. Bang, Y. H. Jung, and S. G. Lee. "The change of bead morphology formed on electrospun polystyrene fibers." *Polymer* 44, no. 14 (2003): 4029-4034.
48. Theron, S. A., E. Zussman, and A. L. Yarin. "Experimental investigation of the governing parameters in the electrospinning of polymer solutions."*Polymer* 45, no. 6 (2004): 2017-2030.
49. Tan, S. H., R. Inai, M. Kotaki, and S. Ramakrishna. "Systematic parameter study for ultra-fine fiber fabrication via electrospinning process." *Polymer* 46, no. 16 (2005): 6128-6134.
50. Gupta, Pankaj, Casey Elkins, Timothy E. Long, and Garth L. Wilkes. "Electrospinning of linear homopolymers of poly (methyl methacrylate): exploring relationships between fiber formation, viscosity, molecular weight and concentration in a good solvent." *Polymer* 46, no. 13 (2005): 4799-4810.
51. Kim, Gil-Tae, Jun-Seok Lee, Jin-Hyouk Shin, Young-Chull Ahn, Yu-Jin Hwang, Hee-Soo Shin, Jae-Keun Lee, and Chang-Mo Sung. "Investigation of pore formation for polystyrene electrospun fiber: effect of relative humidity."*Korean Journal of Chemical Engineering* 22, no. 5 (2005): 783-788.
52. Fong, H., I. Chun, and D. H. Reneker. "Beaded nanofibers formed during electrospinning." *Polymer* 40, no. 16 (1999): 4585-4592
53. Talwar, Sachin, Juan Hinestroza, Benham Pourdeyhimi, and Saad A. Khan. "Associative polymer facilitated electrospinning of nanofibers."*Macromolecules* 41, no. 12 (2008): 4275-4283.

54. *S. Ramakrishna, K. Fujihara, W. E. Teo, T. C. Lim and Z. Ma," An Introduction to Electrospinning and Nanofibers", pp 92, 96, 98, World Scientific Publishing Company, Singapore, 2005.*
55. Hohman, Moses M., Michael Shin, Gregory Rutledge, and Michael P. Brenner. "Electrospinning and electrically forced jets. I. Stability theory."*Physics of Fluids (1994-present)* 13, no. 8 (2001): 2201-2220.
56. Zuo, Weiwei, Meifang Zhu, Wen Yang, and Hao Yu. "Experimental study on relationship between jet instability and formation of beaded fibers during electrospinning." *Polymer Engineering and Science* 45, no. 5 (2005): 704.
57. Shin, Y. M., M. M. Hohman, M. P. Brenner, and G. C. Rutledge. "Electrospinning: A whipping fluid jet generates submicron polymer fibers."*Applied physics letters* 78, no. 8 (2001): 1149-1151.
58. Heikkilä, Pirjo, Lasse Söderlund, Jari Uusimäki, Lauri Kettunen, and Ali Harlin. "Exploitation of electric field in controlling of nanofiber spinning process." *Polymer Engineering and Science* 47, no. 12 (2007): 2065.
59. Han, Tao, Alexander L. Yarin, and Darrell H. Reneker. "Viscoelastic electrospun jets: initial stresses and elongational rheometry." *Polymer* 49, no. 6 (2008): 1651-1658.
60. Helgeson, Matthew E., Kristie N. Grammatikos, Joseph M. Deitzel, and Norman J. Wagner. "Theory and kinematic measurements of the mechanics of stable electrospun polymer jets." *Polymer* 49, no. 12 (2008): 2924-2936.
61. Yarin, A. L., W. Kataphinan, and Darrell Hyson Reneker. "Branching in electrospinning of nanofibers." *Journal of applied physics* 98, no. 6 (2005): 064501.
62. Yu, Jian H., Sergey V. Fridrikh, and Gregory C. Rutledge. "The role of elasticity in the formation of electrospun fibers." *Polymer* 47, no. 13 (2006): 4789-4797.
63. Danielsson, Carina, Sylvie Ruault, Marc Simonet, Peter Neuenschwander, and Peter Frey. "Polyesterurethane foam scaffold for smooth muscle cell tissue engineering." *Biomaterials* 27, no. 8 (2006): 1410-1415.
64. Yannas, I. V., E. Lee, D. P. Orgill, E. M. Skrabut, and G. F. Murphy. "Synthesis and characterization of a model extracellular matrix that induces partial regeneration of adult mammalian skin." *Proceedings of the National Academy of Sciences* 86, no. 3 (1989): 933-937.
65. Griffon, Dominique J., M. Reza Sedighi, David V. Schaeffer, Jo Ann Eurell, and Ann L. Johnson. "Chitosan scaffolds: interconnective pore size and cartilage engineering." *Acta biomaterialia* 2, no. 3 (2006): 313-320.
66. Phipps, Matthew C., William C. Clem, Jessica M. Grunda, Gregory A. Clines, and Susan L. Bellis. "Increasing the pore sizes of bone-mimetic electrospun scaffolds comprised of polycaprolactone, collagen I and hydroxyapatite to enhance cell infiltration." *Biomaterials* 33, no. 2 (2012): 524-534.
67. Karageorgiou, Vassilis, and David Kaplan. "Porosity of 3D biomaterial scaffolds and osteogenesis." *Biomaterials* 26, no. 27 (2005): 5474-5491.
68. Soliman, Sherif, Shilpa Sant, Jason W. Nichol, Masoud Khabiry, Enrico Traversa, and Ali Khademhosseini. "Controlling the porosity of fibrous scaffolds by modulating the fiber diameter and packing density." *Journal of Biomedical Materials Research Part A* 96, no. 3 (2011): 566-574.

69. Ekaputra, Andrew K., Glenn D. Prestwich, Simon M. Cool, and Dietmar W. Hutmacher. "Combining electrospun scaffolds with electrosprayed hydrogels leads to three-dimensional cellularization of hybrid constructs."*Biomacromolecules* 9, no. 8 (2008): 2097-2103.
70. Nerurkar, Nandan L., Sounok Sen, Brendon M. Baker, Dawn M. Elliott, and Robert L. Mauck. "Dynamic culture enhances stem cell infiltration and modulates extracellular matrix production on aligned electrospun nanofibrous scaffolds." *Acta biomaterialia* 7, no. 2 (2011): 485-491.
71. R. A. A. Muzzarelli, *Chitin*, Pergamon Press, Oxford ,UK, 1977.
72. R. A. A. Muzzarelli, C. Jeuniax, and G.W. Gooday, Eds., *Chitin in Nature & Technology*, Plenum Press, New York, NY, USA, 1986.
73. Chen, Z. G., P. W. Wang, B. Wei, X. M. Mo, and F. Z. Cui. "Electrospun collagen–chitosan nanofiber: A biomimetic extracellular matrix for endothelial cell and smooth muscle cell." *Acta Biomaterialia* 6, no. 2 (2010): 372-382.
74. Huang, Chen, Rui Chen, Qinfei Ke, Yosry Morsi, Kuihua Zhang, and Xiumei Mo. "Electrospun collagen–chitosan–TPU nanofibrous scaffolds for tissue engineered tubular grafts." *Colloids and Surfaces B: Biointerfaces* 82, no. 2 (2011): 307-315.
75. Chu, Xue-Hui, Xiao-Lei Shi, Zhang-Qi Feng, Zhong-Ze Gu, and Yi-Tao Ding. "Chitosan nanofiber scaffold enhances hepatocyte adhesion and function."*Biotechnology letters* 31, no. 3 (2009): 347-352.
76. Chen, Jyh-Ping, Shih-Hsien Chen, and Guo-Jyun Lai. "Preparation and characterization of biomimetic silk fibroin/chitosan composite nanofibers by electrospinning for osteoblasts culture." *Nanoscale research letters* 7, no. 1 (2012): 1-11.
77. Mottaghitalab, F., Farokhi, M., Mottaghitalab, V., Ziabari, M., Divsalar, A., & Shokrgozar, M. A. (2011). Enhancement of neural cell lines proliferation using nano-structured chitosan/poly (vinyl alcohol) scaffolds conjugated with nerve growth factor. *Carbohydrate Polymers*, *86*(2), 526-535.
78. Gu, Bon Kang, Sang Jun Park, Min Sup Kim, Chang Mo Kang, Jong-Il Kim, and Chun-Ho Kim. "Fabrication of sonicated chitosan nanofiber mat with enlarged porosity for use as hemostatic materials." *Carbohydrate polymers*97, no. 1 (2013): 65-73.
79. Jayakumar, R., M. Prabaharan, PT Sudheesh Kumar, S. V. Nair, and H. Tamura. "Biomaterials based on chitin and chitosan in wound dressing applications." *Biotechnology advances* 29, no. 3 (2011): 322-337.
80. Paul, Willi, and Chandra P. Sharma. "Chitosan and alginate wound dressings: a short review." *Trends Biomater Artif Organs* 18, no. 1 (2004): 18-23.
81. Kriegel, C., K. M. Kit, D. Julian McClements, and Jochen Weiss. "Electrospinning of chitosan–poly (ethylene oxide) blend nanofibers in the presence of micellar surfactant solutions." *Polymer* 50, no. 1 (2009): 189-200.
82. Duan, Bin, Cunhai Dong, Xiaoyan Yuan, and Kangde Yao. "Electrospinning of chitosan solutions in acetic acid with poly (ethylene oxide)." *Journal of Biomaterials Science, Polymer Edition* 15, no. 6 (2004): 797-811.
83. Jia, Yong-Tang, Jian Gong, Xiao-Hua Gu, Hark-Yong Kim, Jiong Dong, and Xin-Yuan Shen. "Fabrication and characterization of poly (vinyl alcohol)/chitosan blend nanofibers produced by electrospinning method."*Carbohydrate Polymers* 67, no. 3 (2007): 403-409.
84. Van der Schueren, Lien, Iline Steyaert, Bert De Schoenmaker, and Karen De Clerck. "Polycaprolactone/chitosan blend nanofibres electrospun from an acetic acid/formic acid solvent system." *Carbohydrate Polymers* 88, no. 4 (2012): 1221-1226.
85. Shalumon, K. T., K. H. Anulekha, C. M. Girish, R. Prasanth, S. V. Nair, and R. Jayakumar. "Single step electrospinning of chitosan/poly (caprolactone) nanofibers

using formic acid/acetone solvent mixture." *Carbohydrate Polymers* 80, no. 2 (2010): 413-419.
86. Subramanian, Anuradha, David Vu, Gustavo F. Larsen, and Hsin-Yi Lin. "Preparation and evaluation of the electrospun chitosan/PEO fibers for potential applications in cartilage tissue engineering." *Journal of Biomaterials Science, Polymer Edition* 16, no. 7 (2005): 861-873.
87. Pakravan, Mehdi, Marie-Claude Heuzey, and Abdellah Ajji. "A fundamental study of chitosan/PEO electrospinning." *Polymer* 52, no. 21 (2011): 4813-4824.
88. Feng, C., K. C. Khulbe, and T. Matsuura. "Recent progress in the preparation, characterization, and applications of nanofibers and nanofiber membranes via electrospinning/interfacial polymerization." *Journal of Applied Polymer Science* 115, no. 2 (2010): 756-776.
89. Hrůza, J., and J. Poláchová. "Respirator filters with nanofibers." In *5th World Textile Conference AUTEX*, pp. 27-29. 2005.
90. Graham, Kristine, Ming Ouyang, Tom Raether, Tim Grafe, Bruce McDonald, and Paul Knauf. "Polymeric nanofibers in air filtration applications." In*Fifteenth Annual Technical Conference & Expo of the American Filtration & Separations Society, Galveston, Texas*, pp. 9-12. 2002.
91. Grafe, Timothy, Mark Gogins, Marty Barris, James Schaefer, and Ric Canepa. "Nanofibers in filtration applications in transportation." In *Filtration 2001 Conference Proceedings*, pp. 1-15. 2001.
92. Choi, Sung Won, Seong Mu Jo, Wha Seop Lee, and Y-R. Kim. "An electrospun poly (vinylidene fluoride) nanofibrous membrane and its battery applications." *Advanced Materials* 15, no. 23 (2003): 2027-2032.
93. Gopalan, Anantha Iyenger, Padmanabhan Santhosh, Kalayil Manian Manesh, Jin Hee Nho, Sang Ho Kim, Chul-Gyun Hwang, and Kwang-Pill Lee. "Development of electrospun PVdF–PAN membrane-based polymer electrolytes for lithium batteries." *Journal of Membrane Science* 325, no. 2 (2008): 683-690.
94. Yoshimoto, H., Y. M. Shin, H. Terai, and J. P. Vacanti. "A biodegradable nanofiber scaffold by electrospinning and its potential for bone tissue engineering." *Biomaterials* 24, no. 12 (2003): 2077-2082.
95. Bhattarai, Shanta Raj, Narayan Bhattarai, Ho Keun Yi, Pyong Han Hwang, Dong Il Cha, and Hak Yong Kim. "Novel biodegradable electrospun membrane: scaffold for tissue engineering." *Biomaterials* 25, no. 13 (2004): 2595-2602.
96. Tamura, Takuya, and Hiroyoshi Kawakami. "Aligned electrospun nanofiber composite membranes for fuel cell electrolytes." *Nano letters* 10, no. 4 (2010): 1324-1328.
97. Dong, Bin, Liang Gwee, David Salas-de La Cruz, Karen I. Winey, and Yossef A. Elabd. "Super proton conductive high-purity Nafion nanofibers." *Nano letters* 10, no. 9 (2010): 3785-3790.
98. Tehrani, Ashkan Heidarkhan, Ali Zadhoush, Saeed Karbasi, and Hojjat Sadeghi-Aliabadi. "Scaffold percolative efficiency: in vitro evaluation of the structural criterion for electrospun mats." *Journal of Materials Science: Materials in Medicine* 21, no. 11 (2010): 2989-2998.
99. Ziabari, Mohammad, Vahid Mottaghitalab, and Akbar Khodaparast Haghi. "Evaluation of electrospun nanofiber pore structure parameters." *Korean Journal of Chemical Engineering* 25, no. 4 (2008): 923-932.
100. Ghasemi-Mobarakeh, L., D. Semnani, and M. Morshed. "A novel method for porosity measurement of various surface layers of nanofibers mat using image analysis for tissue engineering applications." *Journal of applied polymer science* 106, no. 4 (2007): 2536-2542.

101. Ziabari, Mohammad, Vahid Mottaghitalab, Scott T. McGovern, and A. K. Haghi. "A new image analysis based method for measuring electrospun nanofiber diameter." *Nanoscale Research Letters* 2, no. 12 (2007): 597-600.
102. Salasznyk, Roman M., William A. Williams, Adele Boskey, Anna Batorsky, and George E. Plopper. "Adhesion to vitronectin and collagen I promotes osteogenic differentiation of human mesenchymal stem cells." *BioMed Research International* 2004, no. 1 (2004): 24-34.
103. Yoshimoto, H., Y. M. Shin, H. Terai, and J. P. Vacanti. "A biodegradable nanofiber scaffold by electrospinning and its potential for bone tissue engineering." *Biomaterials* 24, no. 12 (2003): 2077-2082.
104. Ko, Eun Kyoung, Sung In Jeong, Nae Gyune Rim, Young Moo Lee, Heungsoo Shin, and Bu-Kyu Lee. "In vitro osteogenic differentiation of human mesenchymal stem cells and in vivo bone formation in composite nanofiber meshes." *Tissue Engineering Part A* 14, no. 12 (2008): 2105-2119.
105. Ko, Eunkyung, and Seung-Woo Cho. "Biomimetic polymer scaffolds to promote stem cell-mediated osteogenesis." *International journal of stem cells* 6, no. 2 (2013): 87.
106. Li, Wan-Ju, Richard Tuli, Chukwuka Okafor, Assia Derfoul, Keith G. Danielson, David J. Hall, and Rocky S. Tuan. "A three-dimensional nanofibrous scaffold for cartilage tissue engineering using human mesenchymal stem cells." *Biomaterials* 26, no. 6 (2005): 599-609.
107. Caplan, Arnold I., and Scott P. Bruder. "Mesenchymal stem cells: building blocks for molecular medicine in the 21st century." *Trends in molecular medicine* 7, no. 6 (2001): 259-264.
108. Devine, Steven M. "Mesenchymal stem cells: will they have a role in the clinic?." *Journal of Cellular Biochemistry* 85, no. S38 (2002): 73-79.
109. Li, Wan-Ju, Richard Tuli, Xiaoxue Huang, Patrice Laquerriere, and Rocky S. Tuan. "Multilineage differentiation of human mesenchymal stem cells in a three-dimensional nanofibrous scaffold." *Biomaterials* 26, no. 25 (2005): 5158-5166.
110. Hosseinkhani, Hossein, Mohsen Hosseinkhani, Furong Tian, Hisatoshi Kobayashi, and Yasuhiko Tabata. "Osteogenic differentiation of mesenchymal stem cells in self-assembled peptide-amphiphile nanofibers."*Biomaterials* 27, no. 22 (2006): 4079-4086.
111. Cheng, Yixing, Daisy Ramos, Paul Lee, Danni Liang, Xiaojun Yu, and Sangamesh G. Kumbar. "Collagen functionalized bioactive nanofiber matrices for osteogenic differentiation of mesenchymal stem cells: Bone tissue engineering." *Journal of biomedical nanotechnology* 10, no. 2 (2014): 287-298.
112. Polini, Alessandro, Dario Pisignano, Manuela Parodi, Rodolfo Quarto, and Silvia Scaglione. "Osteoinduction of human mesenchymal stem cells by bioactive composite scaffolds without supplemental osteogenic growth factors." *PloS one* 6, no. 10 (2011): e26211.
113. X. Zhang, S. Meng, Y. Huang, M. Xu, Y. He, H. Lin, J. Han, Y. Chai, Y. Wei and X. Deng, Stem Cells Int. 2015 (2015)
114. S. Fujita, H. Shimizu and S. Suye, J. Nanotechnol. 2012 (2012)
115. McBeath, Rowena, Dana M. Pirone, Celeste M. Nelson, Kiran Bhadriraju, and Christopher S. Chen. "Cell shape, cytoskeletal tension, and RhoA regulate stem cell lineage commitment." *Developmental cell* 6, no. 4 (2004): 483-495.
116. Engler, Adam J., Shamik Sen, H. Lee Sweeney, and Dennis E. Discher. "Matrix elasticity directs stem cell lineage specification." *Cell* 126, no. 4 (2006): 677-689.
117. Heo, Su-Jin, Nandan L. Nerurkar, Brendon M. Baker, Jung-Woog Shin, Dawn M. Elliott, and Robert L. Mauck. "Fiber stretch and reorientation modulates mesenchymal stem cell morphology and fibrous gene expression on oriented

nanofibrous microenvironments." *Annals of biomedical engineering* 39, no. 11 (2011): 2780-2790.
118. Gattazzo, Francesca, Anna Urciuolo, and Paolo Bonaldo. "Extracellular matrix: a dynamic microenvironment for stem cell niche." *Biochimica et Biophysica Acta (BBA)-General Subjects* 1840, no. 8 (2014): 2506-2519.
119. Yang, Shoufeng, Kah-Fai Leong, Zhaohui Du, and Chee-Kai Chua. "The design of scaffolds for use in tissue engineering. Part I. Traditional factors."*Tissue engineering* 7, no. 6 (2001): 679-689.
120. Cheng, Ke, and William S. Kisaalita. "Exploring cellular adhesion and differentiation in a micro-/nano-hybrid polymer scaffold." *Biotechnology progress* 26, no. 3 (2010): 838-846.
121. Tuzlakoglu, K., N. Bolgen, A. J. Salgado, Manuela E. Gomes, Erhan Piskin, and R. L. Reis. "Nano-and micro-fiber combined scaffolds: a new architecture for bone tissue engineering." *Journal of Materials Science: Materials in Medicine* 16, no. 12 (2005): 1099-1104.
122. Hussain, Taqadus, Tarun Garg, Amit K. Goyal, and Goutam Rath. "Biomedical applications of nanofiber scaffolds in tissue engineering."*Journal of Biomaterials and Tissue Engineering* 4, no. 8 (2014): 600-623.
123. Liao, Susan, Seeram Ramakrishna, and Murugan Ramalingam. "Development of nanofiber biomaterials and stem cells in tissue engineering." *Journal of Biomaterials and Tissue Engineering* 1, no. 2 (2011): 111-128.
124. Phipps, Matthew C., William C. Clem, Jessica M. Grunda, Gregory A. Clines, and Susan L. Bellis. "Increasing the pore sizes of bone-mimetic electrospun scaffolds comprised of polycaprolactone, collagen I and hydroxyapatite to enhance cell infiltration." *Biomaterials* 33, no. 2 (2012): 524-534.
125. Karageorgiou, Vassilis, and David Kaplan. "Porosity of 3D biomaterial scaffolds and osteogenesis." *Biomaterials* 26, no. 27 (2005): 5474-5491.
126. Soliman, Sherif, Shilpa Sant, Jason W. Nichol, Masoud Khabiry, Enrico Traversa, and Ali Khademhosseini. "Controlling the porosity of fibrous scaffolds by modulating the fiber diameter and packing density." *Journal of Biomedical Materials Research Part A* 96, no. 3 (2011): 566-574.
127. Kazemi Pilehrood, Mohammad, Mandana Dilamian, Mina Mirian, Hojjat Sadeghi-Aliabadi, Laleh Maleknia, Pertti Nousiainen, and Ali Harlin. "Nanofibrous Chitosan-Polyethylene Oxide Engineered Scaffolds: A Comparative Study between Simulated Structural Characteristics and Cells Viability." *BioMed research international* 2014 (2014).
128. Moroni, Lorenzo, Roka Schotel, Doreen Hamann, Joost R. de Wijn, and Clemens A. van Blitterswijk. "3D Fiber-Deposited Electrospun Integrated Scaffolds Enhance Cartilage Tissue Formation." *Advanced Functional Materials* 18, no. 1 (2008): 53-60.
129. Dubas, Stephan T., Paveenuch Kittitheeranun, Ratthapol Rangkupan, Neeracha Sanchavanakit, and Pranut Potiyaraj. "Coating of polyelectrolyte multilayer thin films on nanofibrous scaffolds to improve cell adhesion."*Journal of applied polymer science* 114, no. 3 (2009): 1574-1579.
130. Fatih Canbolat, Mehmet, Christina Tang, Susan H. Bernacki, Behnam Pourdeyhimi, and Saad Khan. "Mammalian cell viability in electrospun composite nanofiber structures." *Macromolecular bioscience* 11, no. 10 (2011): 1346-1356.
131. Sezgin, Mehmet. "Survey over image thresholding techniques and quantitative performance evaluation." *Journal of Electronic imaging* 13, no. 1 (2004): 146-168.
132. Chi, Z., and K. W. Wong. "A two-stage binarization approach for document images." In *Intelligent Multimedia, Video and Speech Processing, 2001. Proceedings of 2001 International Symposium on*, pp. 275-278. IEEE, 2001.

133. Parker, J. R. "Gray level thresholding in badly illuminated images." *IEEE Transactions on Pattern Analysis & Machine Intelligence* 8 (1991): 813-819.
134. Burghardt, Andrew J., Galateia J. Kazakia, and Sharmila Majumdar. "A local adaptive threshold strategy for high resolution peripheral quantitative computed tomography of trabecular bone." *Annals of biomedical engineering*35, no. 10 (2007): 1678-1686.
135. Bieniecki, Wojciech, and Szymon Grabowski. "Multi-pass approach to adaptive thresholding based image segmentation." In *Proceedings of the 8th International IEEE Conference CADSM*, pp. 418-423. 2005.
136. http://fiji.sc/Auto_Local_Threshold, accessed September 2012.
137. Yan, Chen, and Graham Leedham. "Decompose-threshold approach to handwriting extraction in degraded historical document images." In *Frontiers in Handwriting Recognition, 2004. IWFHR-9 2004. Ninth International Workshop on*, pp. 239-244. IEEE, 2004.
138. Blayvas, Ilya, Alfred Bruckstein, and Ron Kimmel. "Efficient computation of adaptive threshold surfaces for image binarization." *Pattern Recognition* 39, no. 1 (2006): 89-101.
139. Sauvola, Jaakko, and Matti Pietikäinen. "Adaptive document image binarization." *Pattern recognition* 33, no. 2 (2000): 225-236.
140. Safinia, Laleh, Athanasios Mantalaris, and Alexander Bismarck. "Nondestructive technique for the characterization of the pore size distribution of soft porous constructs for tissue engineering." *Langmuir* 22, no. 7 (2006): 3235-3242.
141. http://www.nist.gov/lispix/doc/particle-form/morph-param.htm, Accessed September 2012.
142. http://www.sympatec.org/Science/Characterisation/05_ParticleShape.html, Accessed September 2012.
143. Polesel, Andrea, Giovanni Ramponi, and V. John Mathews. "Image enhancement via adaptive unsharp masking." *IEEE transactions on image processing* 9, no. 3 (2000): 505-510.
144. Ramponi, Giovanni, Norbert K. Strobel, Sanjit K. Mitra, and Tian-Hu Yu. "Nonlinear unsharp masking methods for image contrast enhancement."*Journal of Electronic Imaging* 5, no. 3 (1996): 353-366.
145. Polesel, Andrea, Giovanni Ramponi, and V. John Mathews. "Adaptive unsharp masking for contrast enhancement." In *Image Processing, 1997. Proceedings., International Conference on*, vol. 1, pp. 267-270. IEEE, 1997.
146. Narendra, Patrenahalli M. "A separable median filter for image noise smoothing." *Pattern Analysis and Machine Intelligence, IEEE Transactions on* 1 (1981): 20-29.
147. Jagatheeswari, P., S. Suresh Kumar, and M. Rajaram. "Contrast enhancement for medical images based on histogram equalization followed by median filter." (2009).
148. http://www.graphpad.com, accessed September 2012.
149. Heikkilä, Pirjo, Aimo Taipale, Matti Lehtimäki, and Ali Harlin. "Electrospinning of polyamides with different chain compositions for filtration application." *Polymer Engineering & Science* 48, no. 6 (2008): 1168-1176.
150. Bruil, Anton, Tom Beugeling, and Jan Feijen. "A mathematical model for the leukocyte filtration process." *Biotechnology and bioengineering* 45, no. 2 (1995): 158-164.
151. Kalayci, Veli, Ming Ouyang, and Kristine Graham. "Polymeric nanofibres in high efficiency filtration applications." *FILTRATION-COALVILLE*- 6, no. 4 (2006): 286.
152. Wang, Hwa-Chi, and Gerhard Kasper. "Filtration efficiency of nanometer-size aerosol particles." *Journal of Aerosol Science* 22, no. 1 (1991): 31-41.

153. Abràmoff, Michael D., Paulo J. Magalhães, and Sunanda J. Ram. "Image processing with ImageJ." *Biophotonics international* 11, no. 7 (2004): 36-42.
154. Motulsky, Harvey, and Arthur Christopoulos. *Fitting models to biological data using linear and nonlinear regression: a practical guide to curve fitting*. Oxford University Press, 2004.
155. Sadeghi-Aliabadi, H., M. Aliasgharluo, A. Fattahi, M. Mirian, and M. Ghannadian. "In vitro cytotoxic evaluation of some synthesized COX-2 inhibitor derivatives against a panel of human cancer cell lines." *Research in pharmaceutical sciences* 8, no. 4 (2013): 298.
156. Shenoy, Suresh L., W. Douglas Bates, Harry L. Frisch, and Gary E. Wnek. "Role of chain entanglements on fiber formation during electrospinning of polymer solutions: good solvent, non-specific polymer–polymer interaction limit." *Polymer* 46, no. 10 (2005): 3372-3384.
157. Ra, Eun Ju, Kay Hyeok An, Ki Kang Kim, Seung Yol Jeong, and Young Hee Lee. "Anisotropic electrical conductivity of MWCNT/PAN nanofiber paper."*Chemical Physics Letters* 413, no. 1 (2005): 188-193.
158. Mazinani, Saeedeh, Abdellah Ajji, and Charles Dubois. "Morphology, structure and properties of conductive PS/CNT nanocomposite electrospun mat." *Polymer* 50, no. 14 (2009): 3329-3342.
159. Vaisman, Linda, Ellen Wachtel, H. Daniel Wagner, and Gad Marom. "Polymer-nanoinclusion interactions in carbon nanotube based polyacrylonitrile extruded and electrospun fibers." *Polymer* 48, no. 23 (2007): 6843-6854.
160. Sung, Jun Hee, Hyun Suk Kim, Hyoung-Joon Jin, Hyoung Jin Choi, and In-Joo Chin. "Nanofibrous membranes prepared by multiwalled carbon nanotube/poly (methyl methacrylate) composites." *Macromolecules* 37, no. 26 (2004): 9899-9902.
161. *G. Wypych," Hand Book of Plasticizer", pp 108-110, ChemTec Publishing, Toronto, 2004.*
162. Wunderlich, T., M. Stelter, T. Tripathy, B. R. Nayak, G. Brenn, A. L. Yarin, R. P. Singh, P. O. Brunn, and F. Durst. "Shear and extensional rheological investigations in solutions of grafted and ungrafted polysaccharides." *Journal of applied polymer science* 77, no. 14 (2000): 3200-3209.
163. Wang, M., A. J. Hsieh, and G. C. Rutledge. "Electrospinning of poly (MMA-co-MAA) copolymers and their layered silicate nanocomposites for improved thermal properties." *Polymer* 46, no. 10 (2005): 3407-3418.
164. Balguid, Angelique, Anita Mol, Mieke H. van Marion, Ruud A. Bank, Carlijn VC Bouten, and Frank PT Baaijens. "Tailoring fiber diameter in electrospun poly (ε-caprolactone) scaffolds for optimal cellular infiltration in cardiovascular tissue engineering." *Tissue Engineering Part A* 15, no. 2 (2008): 437-444.
165. Sell, Scott, Catherine Barnes, David Simpson, and Gary Bowlin. "Scaffold permeability as a means to determine fiber diameter and pore size of electrospun fibrinogen." *Journal of Biomedical Materials Research Part A* 85, no. 1 (2008): 115-126.
166. Pham, Quynh P., Upma Sharma, and Antonios G. Mikos. "Electrospun poly (ε-caprolactone) microfiber and multilayer nanofiber/microfiber scaffolds: characterization of scaffolds and measurement of cellular infiltration."*Biomacromolecules* 7, no. 10 (2006): 2796-2805.
167. Moroni, L., J. R. De Wijn, and C. A. Van Blitterswijk. "3D fiber-deposited scaffolds for tissue engineering: influence of pores geometry and architecture on dynamic mechanical properties." *Biomaterials* 27, no. 7 (2006): 974-985.
168. Pilehrood, Mohammad Kazemi, and Pirjo Heikkil. "Simulation of structural characteristics and depth filtration elements in interconnected nanofibrous membrane based on adaptive image analysis." *World Journal of Nano Science and Engineering* 2013 (2013).

169. Badami, Anand S., Michelle R. Kreke, M. Shane Thompson, Judy S. Riffle, and Aaron S. Goldstein. "Effect of fiber diameter on spreading, proliferation, and differentiation of osteoblastic cells on electrospun poly (lactic acid) substrates." *Biomaterials* 27, no. 4 (2006): 596-606.
170. Sisson, Kristin, Chu Zhang, Mary C. Farach-Carson, D. Bruce Chase, and John F. Rabolt. "Fiber diameters control osteoblastic cell migration and differentiation in electrospun gelatin." *Journal of Biomedical Materials Research Part A* 94, no. 4 (2010): 1312-1320.
171. Santos, Marina I., Kadriye Tuzlakoglu, Sabine Fuchs, Manuela E. Gomes, Kirsten Peters, Ronald E. Unger, Erhan Piskin, Rui L. Reis, and C. James Kirkpatrick. "Endothelial cell colonization and angiogenic potential of combined nano-and micro-fibrous scaffolds for bone tissue engineering."*Biomaterials* 29, no. 32 (2008): 4306-4313.
172. Christopherson, Gregory T., Hongjun Song, and Hai-Quan Mao. "The influence of fiber diameter of electrospun substrates on neural stem cell differentiation and proliferation." *Biomaterials* 30, no. 4 (2009): 556-564.
173. Hinnebusch, Brian F., Aleem Siddique, J. Welles Henderson, Madhu S. Malo, Wenying Zhang, Christopher P. Athaide, Mario A. Abedrapo, Xinming Chen, Vincent W. Yang, and Richard A. Hodin. "Enterocyte differentiation marker intestinal alkaline phosphatase is a target gene of the gut-enriched Krüppel-like factor." *American Journal of Physiology-Gastrointestinal and Liver Physiology* 286, no. 1 (2004): G23-G30.
174. Matsumoto, Hisashi, Roger H. Erickson, James R. Gum, Masahiro Yoshioka, Elizabeth Gum, and Young S. Kim. "Biosynthesis of alkaline phosphatase during differentiation of the human colon cancer cell line Caco-2." *Gastroenterology* 98, no. 5 (1990): 1199-1207.
175. Viereck, Volker, Heide Siggelkow, Simone Tauber, Dirk Raddatz, Norbert Schutze, and Michael Hüfner. "Differential regulation of Cbfa1/Runx2 and osteocalcin gene expression by vitamin-D3, dexamethasone, and local growth factors in primary human osteoblasts." *Journal of cellular biochemistry* 86, no. 2 (2002): 348-356.
176. Seyedjafari, Ehsan, Masoud Soleimani, Nasser Ghaemi, and Iman Shabani. "Nanohydroxyapatite-coated electrospun poly (l-lactide) nanofibers enhance osteogenic differentiation of stem cells and induce ectopic bone formation."*Biomacromolecules* 11, no. 11 (2010): 3118-3125.
177. Ho, Ming-Hua, Mei-Hsiu Liao, Yi-Ling Lin, Chien-Hao Lai, Pei-I. Lin, and Ruei-Ming Chen. "Improving effects of chitosan nanofiber scaffolds on osteoblast proliferation and maturation." *International journal of nanomedicine*9 (2014): 4293.
178. Hawse, J. R., M. Subramaniam, J. N. Ingle, M. J. Oursler, N. M. Rajamannan, and T. C. Spelsberg. "Estrogen-TGFβ cross-talk in bone and other cell types: Role of TIEG, Runx2, and other transcription factors."*Journal of cellular biochemistry* 103, no. 2 (2008): 383-392.
179. Ho, Wei-Pin, Wing-Pong Chan, Ming-Shium Hsieh, and Ruei-Ming Chen. "Runx2-mediated bcl-2 gene expression contributes to nitric oxide protection against hydrogen peroxide-induced osteoblast apoptosis." *Journal of cellular biochemistry* 108, no. 5 (2009): 1084-1093.
180. Ardeshirylajimi, Abdolreza, Saman Hosseinkhani, Kazem Parivar, Parichehr Yaghmaie, and Masoud Soleimani. "Nanofiber-based polyethersulfone scaffold and efficient differentiation of human induced pluripotent stem cells into osteoblastic lineage." *Molecular biology reports* 40, no. 7 (2013): 4287-4294.
181. K. L. Moffat, M. B. Boushell, X. Zhang, W.N. Levine and H. H. Transactions of the Orthopaedic Research Society Annual Meeting, 2011, Long Beach, CA.

182. Barberá, M. José, Agatha Schlüter, Neus Pedraza, Roser Iglesias, Francesc Villarroya, and Marta Giralt. "Peroxisome Proliferator-activated Receptor α Activates Transcription of the Brown Fat Uncoupling Protein-1 Gene A LINK BETWEEN REGULATION OF THE THERMOGENIC AND LIPID OXIDATION PATHWAYS IN THE BROWN FAT CELL." *Journal of Biological Chemistry* 276, no. 2 (2001): 1486-1493.
183. Zhau, Haiyen E., Hui He, Christopher Y. Wang, Majd Zayzafoon, Colm Morrissey, Robert L. Vessella, Fray F. Marshall, Leland WK Chung, and Ruoxiang Wang. "Human prostate cancer harbors the stem cell properties of bone marrow mesenchymal stem cells." *Clinical Cancer Research* 17, no. 8 (2011): 2159-2169.
184. Tai, Tzu-Ann C., Caroline Jennermann, Kathleen K. Brown, Beverly B. Oliver, Marissa A. MacGinnitie, William O. Wilkison, H. Roger Brown et al. "Activation of the nuclear receptor peroxisome proliferator-activated receptor γ promotes brown adipocyte differentiation." *Journal of Biological Chemistry*271, no. 47 (1996): 29909-29914.
185. Sears, Irina B., Marissa A. MacGinnitie, Laszlo G. Kovacs, and Reed A. Graves. "Differentiation-dependent expression of the brown adipocyte uncoupling protein gene: regulation by peroxisome proliferator-activated receptor gamma." *Molecular and cellular biology* 16, no. 7 (1996): 3410-3419.

SUMMARIES OF PAPERS

In paper I, polyacrylonitrile (PAN) nanofibers and carbon nanotube (CNT) reinforced PAN nanofiber were successfully electrospun. Ethylene carbonate (EC) as polymer plasticizer was added into PAN/CNT solutions. The average diameter of fibers varied from 80 to 240 nm. The study investigated the effects of polymer concentration, CNT and EC on morphological characteristics of electrospun PAN fibers. Electrospinning parameters were set in constant value to prevent their mutual influences on resultant morphology. It was observed that increasing polymer concentration led to reduction of beads density and increased diameter of PAN nanofibers. The fiber diameters were increased by addition of CNTs below electrical percolation threshold. In particular, it was found that the inclusion of EC enables changes in morphological characteristic of PAN/CNT nanocomposite fiber regardless of its conductivity and viscosity impacts.

In paper II, the structural characteristics of electrospun membranes were quantified by introducing a rigorous image analysis technique and were used to evaluate the permeation–filtration mechanism. To this end, a nanostructured fibrous network was simulated as an ideal membrane using adaptive local criteria in the image analysis. The reliability of the proposed approach was validated with measurements and comparison of structural characteristics in different morphological conditions. The results were found to be well compatible with empirical observations of perfect membrane structures. This approach, based on optimization of electrospinning parameters, may pave the way for producing optimal membrane structures for boosting the performance of electrospun membranes in end-use applications.

In paper III, 3D nanofibrous chitosan-polyethylene oxide (PEO) scaffolds were fabricated by electrospinning at different processing parameters. The structural characteristics, such as pore size, overall porosity, pore interconnectivity and scaffold percolative efficiency (SPE), were simulated by a robust image analysis. Mouse fibroblast cells (L929) were cultured in RPMI for 2 days in presence of various samples of nanofibrous chitosan/PEO scaffolds. Cell attachments and corresponding mean viability were enhanced from 50% to 110% compared to that belonging to a control even at packed morphologies of scaffolds composed of pores with nanoscale diameter. To elucidate the correlation between structural characteristics within the depth of the scaffolds' profile and cell viability, a comparative analysis was proposed. This analysis revealed that larger fiber diameters and pore sizes can enhance cell viability. On the contrary, increasing the other structural elements such as overall porosity and interconnectivity can reduce the viability of cells due to a simultaneous reduction in fiber diameter and pore size through the electrospinning process. In addition, it was found that manipulation of the processing parameters in electrospinning can compensate for the effects of packed morphologies of nanofibrous scaffolds, and can thus potentially improve the infiltration and viability of cells.

In paper IV, a new hybrid scaffold constructed by coating electrospun chitosan/polyethylene oxide (PEO) nanofibers on commercial BioTek polystyrene (PS) scaffold obtained from Sigma Aldrich was presented. The viability and proliferation rate of mesenchymal stem cells (MSCs) seeded on micro-nano structured hybrid scaffold (MNHS) and commercial PS scaffolds were analyzed by MTT assay. The results of MTT assay revealed a higher degree of viability and proliferation rate in MSCs seeded on MNHS compared with commercial PS scaffold. DAPI images also confirmed the higher degree of attachment and viability of MSCs seeded on MNHS. Moreover, MSCs on both scaffolds differentiated to osteoblasts and adipocytes cells, as reflected by the images obtained from Alizarin Red and Oil Red-O staining. Alkaline phosphatase activity (ALP) and calcium content assays revealed that the MNHS has a higher potential for osteogenic differentiation than the commercial scaffold. To quantify the osteoblast and adipocyte gene expression, quantitative RT-PCR was carried out for MNHS, commercial scaffold and Tissue culture polystyrene (TCPS). It was found that MNHS can express a higher level of Runt-related transcription factor 2 (Runx2), osteonectin and osteocalcin in osteogenic differentiation as well as increased expression of PPARγ and UCP-1 in adipogenic differentiation. The enhancement of attachment, viability and proliferation as well as bi-lineage differentiation may result from biochemical and structural analogies of MNHS to native ECM. Furthermore, it was observed that biocompatible MNHS scaffold can potentially be utilized as a suitable scaffold for bone and connective tissue engineering.

Paper I

PREPARATION OF CARBON NANOTUBE EMBEDDED IN POLYACRYLONITRILE (PAN) NANOFIBRE COMPOSITES BY ELECTROSPINNING PROCESS

Mohammad Kazemi Pilehrood, Pirjo Heikkilä and Ali Harlin
AUTEX Research Journal, 2012, 12, 1-6

Paper II

Simulation of Structural Characteristics and Depth Filtration Elements in Interconnected Nanofibrous Membrane Based on Adaptive Image Analysis

Mohammad Kazemi Pilehrood, Pirjo Heikkilä and Ali Harlin

World Journal of Nano Science and Engineering, 2013, 3, 6-16

Paper III

Nanofibrous Chitosan-Polyethylene Oxide Engineered Scaffolds: A Comparative Study between Simulated Structural Characteristics and Cells Viability

Mohammad Kazemi Pilehrood, Mandana Dilamian, Mina Mirian, Hojjat Sadeghi-Aliabadi, Laleh Maleknia, Pertti Nousiainen and Ali Harlin

BioMed Research International, Volume 2014 (2014), Article ID: 438065

Paper IV

3D Micro-Nano Structured Hybrid Scaffolds: An Investigation Into the Role of Nanofiber Coating on Viability, Proliferation and Differentiation of Seeded Mesenchymal Stem Cells

Mohammad Kazemi Pilehrood, Amir Atashi, Hojjat Sadeghi-Aliabadi, Pertti Nousiainen and Ali Harlin

Journal of Nanoscience and Nanotechnology, 2016, 16, 9000-9007

Tampereen teknillinen yliopisto
PL 527
33101 Tampere

Tampere University of Technology
P.O.B. 527
FI-33101 Tampere, Finland

ISBN 978-952-15-3843-8
ISSN 1459-2045